Simulation of the deformation of a stope support design

AJ Laubscher

20228732

Dissertation submitted in fulfilment of the requirements for the degree *Magister in Mechanical Engineering* at the Potchefstroom Campus of the North-West

Supervisor	Prof. J. Markgraaff
Co-Supervisor	Dr. C.B. Nel

May 2014

Uitreksel

Een van die mees algemene mynmetodes in moderne diepvlak-goudmynbou is gesteunde *werkplek* uitgrawings. Die werkplekke, waar erts uitgegrawe word, word ondersteen deur ‘n kombinasie van hang-boute, hout pakke, *Backfill*, hout stutte en meganiese tipes stutte. Vir hierdie steun stelsels om effektief te wees in hul funksie om die hang te ondersteun en terselfdetyd die energie te absorbeer wat gedurende die elastiese vervorming van die rots massa plaasvind, is dit nodig dat die rots-ingenieur moet weet hoe elke tipe stut op die uitsetting van die omringende rotsmassa reageer. Hierdie reaksie, ook genoem *die prestasie van die sisteem*, word deur die vervaardiger van stuttipes in aanmerking geneem tydens die oorweging van stuttegnologie, die vereiste spesifikasie en die ontwerp van die stut.

Die ontwikkeling van steunstelsels word tans gedoen met behulp van kennis-uit-ondervinding en deur middel van tydrowende en duur iteratiewe *trap-en-tref* metodes.

‘n Studie is gedoen om te bepaal wat die gangbaarheid van *Eindige Element Modelering (EEM)* is om die vervorming van ‘n moderne steunstut te simuleer onder gespesifiseerde *kwasi-statiese* en *dinamiese* toestande met die doel om die operasionele prestasie van die stut te voorspel na aanleiding van die gebrek aan toetsvasaliteite, -vaardighede en –toerusting. Hierdie studie is verder gevoer deur middel van modelering en berekeninge om die moontlikheid van knik as gevolg van ‘n impakbelading van 3m/s, geassosieer met ondergrondse mynbou geinduseerde seismiese aktiwiteit, te bepaal asook die effek wat dit het op die prestasie van ‘n kommersiëel-beskikbare stuttipe.

Om bogenoemde te bepaal is simulasies met behulp van *ANSYS™ Transient Structural* sagteware uitgevoer en gerekenariseerde prosedures was toegepas met behulp van knik teorie om the bepaal wat die moontlikhied van faling as gevolg van knik, is.

Uit die resultate van hierdie studie is getoon dat dit moontlik is om die prestasie-kurwe vir ‘n meganiese wrywings-tipe stut te simuleer en die resultate te vergelyk met die prestasie wat van die ontwerp vereis word, gegewe dat die *wrywingsfaktor* bekend is. ‘n Metode word aangebied om die teoretiese potensiaal van knik as gevolg van hoë-snelheid-impak-beladings op wrywings-tipe stutte, en slank-stutte in die algemeen, te ondersoek en te bepaal.

Die metodologie wat gebruik is in die studie, kan toegepas word op verskillende stut-ontwerpe om die ontwikkelingstyd en koste van implementering daarvan te verlaag.

Abstract

Supported stope mining is one of the most common types of mining in the modern day gold mining industry. The excavated regions, where ore is extracted, are supported with a combination of roof-bolting, timber packs, backfill, timber props and mechanical prop technologies. In order to install a support system that will be able to absorb the energy released by the elastic movement of the surrounding rock mass and support the unstable hanging wall, it is necessary for the rock engineer to know how the individual types of support will react to different load conditions in order to design a safe support system.

Current support systems are developed using knowledge from past experience and trial and error processes. These are expensive and time consuming methods that can possibly be improved and made more cost effective by using modern design techniques.

A study was conducted to determine the feasibility of the application of Finite Element Modelling (FEM) to the deformation of a modern support unit under specified *quasi-static* and *dynamic* stope load conditions with the view to assist in the prediction of the operational performance of support units that cannot be experimentally tested due to a lack of test equipment, capabilities and facilities. The study was extended by investigating the theoretical possibility of buckling due to an impact load on the prop and the performance of the prop. To achieve this, a simulation was carried out using *ANSYS™* transient structural software to determine whether it is possible to simulate the performance curve of a prop. Computerised methods were used to determine the possibility of failure due to buckling and the implications of buckling, if it occurs, on the performance of a specific support prop design.

In summary this study proved that it is possible to simulate the performance curve of a friction prop design in order to compare the result obtained with the required performance, provided that the correct friction coefficients between prop mating surfaces are known. It also presents a methodology to investigate the theoretical effect of high velocity impact load on the buckling potential of a friction prop design and slender columns in general, which is highly applicable to these types of support.

The methodologies used in this study can be applied to different designs of friction props, and possibly reduce the development costs and implementation time of these types of support units.

Keywords

Stope support prop

Finite Element Analyses

Buckling

Impact loading

Non-linear Material Behaviour

Friction

Acknowledgements

A number of role players are to be acknowledged for fulfilling key functions in the successful deliverance of this dissertation.

Mine Support Products (MSP): **MSP** chose the *North West University - School for Mechanical Engineering* as the research platform to execute this study on the Rockprop MK 2 manufactured by them. They provided funding, test results and general vital information and support that was key to the successful deliverance of this dissertation.

Prof. Johann Markgraaff: Prof. J. Markgraaff was the supervisor of this study. He ensured that research of a high quality was maintained and delivered throughout the course of this study. I thank him for his willingness to lead the study and to accommodate and guide me.

Dr. Carel B. Nel: Dr. C.B. Nel provided indispensable technical inputs that ensured a high quality and comprehensive research product. I thank him for fulfilling the role of Co-supervisor and his valuable time to review and guide the content of this dissertation with respect to the buckling analyses.

Mr. Christiaan Nissen: Mr. C. Nissen is the design engineer at **MSP** and was the facilitator of this study. He is thanked for his support and open line of communication throughout the study.

A note:

Prof. Markgraaff; nogmaals dankie dat u bereid was om my onbepland te akkomodeer tenspyte van ‘n vol en besige skedule. Dit was van onskatbare waarde vir my en ‘n groot voorreg!

Dr. Nel; ek is baie dankbaar vir u insette en hoë-vlak leiding. Dit was werklik ‘n plesier en voorreg om saam met u te kon werk.

Aan my ouers, broer en susters; Dankie vir jul deurlopende ondersteuning (geestelik, emosioneel en finansieel)!

> *“God gave the day, God gave the strength for it. And that day and the strength were consecrated to labour, and that labour was its own reward” Tolstoy; Anna Karenina*

Alle eer en verheerliking aan God, want dit is Hy wat die avontuur van die lewe skenk en onderhou!

Contents

List of Figures

List of Tables

Acronyms and Abbreviations

Acronym	Description
FEA	Finite Element Analysis
FOG	Fall of Ground
ERR	Energy Release Rate
ESR	Strain Energy Storage Rate
kN	Kilo-Newton
m	Meter
kg	Kilogram
s	Second
mm	Millimetre
FOS	Factor of Safety
UTS	Ultimate Tensile strength
ANSYS™	ANSYS™ 13.0 Academic Version
MATLAB™	MATLAB version 7.10 r2010a
MSP	Mine Support Products
FEM	Finite Element Method
EES	Engineering Equation Solver
ODE	Ordinary Differential Equation
ODE23	Ordinary Differential Equation Solver for second and third order differential equations (Routine in MATLAB)
EPPM	Elastic-Perfectly Plastic Model
AISI	American Iron and Steel Institute

Nomenclature

Symbol	Description	Unit
A_T	Potential Tributary Area	m^2
F	Support Unit Load; Force	N
g	Earth gravitational acceleration	m/s^2
ρ_r	Rock density	kg/m^3
b	Height of instability	m
E_A	Energy absorption capacity	kJ
m	Mass	Kg
v	Velocity	m/s
h	Vertical displacement of hanging-wall	M
σ_i	Normal stress in i-direction	Pa
τ_i	Shear stress in i-direction	Pa
E	Young's Modulus	Pa
E_{Tan}	Tangent Modulus	Pa
ε	Strain	%
σ_U	Ultimate tensile strength	Pa
σ_Y, Sy	Yield limit	Pa
ε_{fail}	Failure Strain	Pa
ε_{proof}	Proof strain	%
P	Contact Pressure	Pa
$COHE$	Shear stress at which sliding on surface begins	Pa
$TAUMAX$	Maximum contact friction	Pa
μ	Coefficient of friction	
MU	Dynamic Coefficient of friction	
$FACT$	Ratio of static to dynamic coefficient of friction	

DC	Decay Coefficient	
v_{rel}	Relative slip rate between surfaces	m/s
μ_s	Static coefficient of friction	
P_{cr}	Critical buckling load on a columnar member	N
I	Second moment of inertia of aria	m^4
L	Length of a column	m
l	Coordinate along length of column	m
σ_{cr}	Critical buckling stress	Pa
A	Cross sectional Area of a column	m^2
ρ	Radius of gyration of a column	m
L_{eff}	Effective length of a supported column	m
$F(t)$	Time dependant Force function	N
c	Viscous damping coefficient	N/m/s
k	Stiffness/ spring coefficient	N/m
$x,$	Displacement	m
$\dot{x}$	Velocity	m/s
$\ddot{x}$	Acceleration	m/s^2
ω_n	Natural Frequency	Hz
c_c	Critical damping coefficient	N/m/s
ζ	Damping ratio	
El	Elongation percentage	%
x_s	Deformation	m
y	Maximum horizontal distance	m
$y(x)$	Horizontal coordinate	m

CHAPTER 1 Introduction

Deep level mining forms a substantial part of the mining industry in South Africa. The support of haulages and mining excavations in such mines are the most important mechanism to prevent fatal injuries, damaged and lost equipment and production losses due to rock falls. This section gives a brief overview and background on this topic and its relevance to the current study.

1.1 Supported Mining

Supported stope mining is one of the most important and critical processes in the mining of gold. The stopes are the areas in underground mines where ore containing rock is extracted from the rock mass. Mining activities such as these cause geometric and stress level (energy balance) changes in the surrounding rock mass. The energy balance, which in effect is the difference between the stored energy and the energy that can be dissipated, is rearranged in the new geometry profile and a new energy profile is formed around the excavated region. This rearrangement of the energy profile in the new geometry is associated with rock mass expansion through elastic deformation or brittle failure which may be accompanied by catastrophic and violent rock bursts or rock displacement, that lead to closure of the excavated region.

Consequently, the phenomenon of stope closure poses a great threat to efficient production, safety of workers and equipment. For this reason the control of ground movement and the convergence/closure rate of the hanging and the foot wall that occurs in the excavated regions, is an essential part of stoping, stope support and its design.

In modern day applications ground control systems consists of combinations of timber packs, roof-bolting, timber props, backfill, tendons, composite packs and mechanical prop technologies.

Authors such as Daehnke *et al.* (2001) developed testing procedures to define stope support specifications that are used in current South African supported stope processes. These performance specifications of support units are required by rock engineers to be able to design and apply support systems for specific stoping environments. To obtain the performance specification of a specific type of support, multiple units are subjected to laboratory tests and *in-situ* performance data recordings. These results are combined to define the final performance specification that can be used in support systems and support design phases. Because of the variability in the mechanical properties of timber types of support and other designs made from non-uniform materials, it is required that the multiple units be tested on a

regular bases to continuously update the performance specification of the specific types of support designs.

1.2 Problem Statement and Aim of the Study

One attempt to solve the problem of variable performance delivery of support units is to use mechanical support units that are made from materials that behave uniformly and predictably. To determine and verify the performance characteristics of a design however, it is still required that multiple units of the specific design are subjected to a range of full scale laboratory and field tests, accompanied by empirical and statistical approaches.

These tests and approaches are however time consuming and expensive. Furthermore, test equipment presently available is limited with respect to their range in obtainable closure rate and maximum load settings. These obstacles have application cost implications and also seriously limit the development of support units that can cope with the high deformation rates that typically occur during rock bursts and other seismic events. Dynamic loading conditions, such as seismic events, will also have a definite effect on the buckling of the support columns and thus their performance.

It is thought that computer simulation of the deformation of support unit designs under specified *dynamic* and *quasi-static* loading conditions, similar to those experienced in stoping environments, can reduce the cost and the physical effort to develop, test and improve on the performance characteristics of existing or required support units.

Finite Element Analyses (FEA) systems are computerized simulation software used in the design cycle to simulate and predict the behaviour of complex systems, and to optimize designs based on these predictions.

The aim of this study is to:

1. Review the design base of support prop design, design principles and performance requirements;
2. Review the application of computer simulation to stope support design;
3. Determine the feasibility of the application of *Finite Element Modelling (FEM)* to the deformation of a modern support design under specified *quasi-static* and *dynamic* stope load conditions with the view to assist in the prediction of the operational performance of support units that cannot be experimentally tested due to a lack of test equipment capabilities and facilities;
4. Determine the theoretical potential of buckling on a stope support design and the implications that buckling may have on the performance of a specific commercially available support prop design.

CHAPTER 2 Literature Review

This study is a result of an ongoing campaign in the mining industry to improve the safety of employees in the stoping areas. As a result mining groups are committed to investment in sustainable and effective support systems.

Companies that supply support systems for stoping purposes are constantly challenged to improve their products to be able to provide a competitive product. To be able to improve their products it is necessary to understand mining and the behaviour of rock around excavated regions. This combined with a broad and comprehensive understanding of the engineering concepts and technologies involved, such as material behaviour and *FEM* technologies, is paramount to improving and optimizing current designs.

Chapter 2 reviews this background and presents a broad overview on research that was done to date to optimize the design of a support prop. Furthermore it reviews the theory behind methods that are used to do computerized *FEM* simulations of material behaviour and mechanical interactions that may be applied to the design stage of support prop.

2.1 Background

Fall Of Ground (FOG) incidents are still a major concern in modern underground mining, and a continuous threat to production and the safety of personnel. This phenomenon led to studies and tests to predict the performance of support units in the stoping environment. The first step in further application of such technologies was to quantify the *load-reaction/load-deformation* of the support systems then employed so that performance variables would provide for the rock mechanics involved.

Ground closure and rock movement have been explained by way of two main behavioural characteristics. The first is the elastic movement of ground, which refers to slow closure rates appropriately named *quasi-static behaviour*. The second behaviour is defined as *dynamic behaviour* which refers to fluctuating behaviour of rock mass caused by mining induced release of stress or externally induced seismic activities that can give rise to brittle failure of the rock mass and violent rock bursts. (Ortlepp, 1983).

Daehnke *et al* (2001) present values for *quasi-static* and *dynamic* closure conditions based on measurements from previous studies. For *quasi-static* conditions a closing rate value of 30mm/minute was defined and even though *dynamic* conditions are associated with violent fluctuating behaviour, a value of 3m/s closing rate was defined for testing purposes.

Several techniques have been developed to assess the rock-burst potential of underground mining excavations. Some of these techniques use the energy balance around the excavated

regions to calculate the energy that is available for rock-burst situations. The phenomena of movement due to energy release are quantified by *Energy Release Rate* (*ERR*) and strain *Energy Storage Rate* (*ESR*) which describes the strain energy storage rate (Cook *et al.*, 1966:435). Energy balance calculations based on elastic behaviour of the overhead rock mass and the support thereof were reviewed in detail by Salamon (1970, 1974, 1983, 1984), Walsh (1977), Budavari (1983), Brady and Brown (1985), McMahon (1988) and Medley (1992).

2.1.1 Rock Mass Parameters in Stope Support Design

Stope support design criterion, such as those discussed by Wagner (1984) for rockburst prone mines, takes the kinetic and potential energy of the mine key-blocks[1] into account to determine the support requirements for the excavated regions. The concept of *support resistant force per unit surface*, which forms the base for the '*tributary area design criterion',* is explained in detail by Wagner(1984). The *tributary area methodology* is currently used by Rock mechanic specialists in the South African gold and platinum mines to design stope support systems.

The tributary area analysis is used to determine the weight of rock mass that needs to be supported in a certain underground environment. The area is determined by the face layout and the height of potential fall, which is assumed to be known from collected data. This area is then divided into a fixed number of support units to determine the support layout. This relationship is expressed as:

$$A_T = \frac{F}{\rho g b} \qquad (2.1)$$

where: A_T = maximum potential tributary area (m^2)

F = support unit load (N)

ρ = rock density (kg/m^3)

g = acceleration due to gravity (10 m/s^2)

b = height of instability (m)

The relationship between these variables is illustrated in Figure 2.1.

Figure 2.1 presents the amount of area that a single support unit with a specific *load capacity* can carry for a given height of instability. (Daehnke *et al.*, 2001:135.)

[1] Unstable blocks of rock surrounding an excavated region, which is formed because of geological joints, fractures or mining induced fractures.

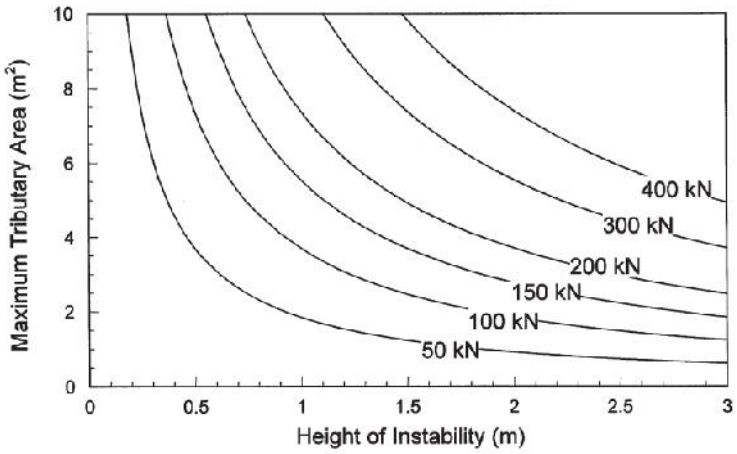

Figure 2.1: Energy absorption requirements for the Tributary Area Analyses (after Daehnke, A. 2001)

The approach taken for rock burst events is based on the energy absorption capacity E_A, of the support unit and is given by (Wagner, 1984:209.), as

$$E_A = 0.5mv^2 + mgh \qquad (2.2)$$

where: $m = \rho g A_t$.

This relationship can be re-written as:

$$A_T = \frac{E_A}{\circ b\left(0.5v^2 + gh\right)} \qquad (2.3)$$

where: A_T = Maximum potential tributary area (m^2)

b = height of instability (m)

E_A = Energy absorption capacity of the support (J)

ρ = Rock mass density (kg/m^2)

v = Rock ejection velocity (3m/s)

g = Acceleration due to gravity ($10m/s^2$)

h = Vertical displacement of hanging-wall during dynamic events (0.2m)[2]

[2] The general assumption is that the displacement is 0.2m. In reality closure is dependent on the reaction force of the support prop and is less than 0.2m for most support systems.

The *zone of support influence* and *stability analyses* considers the buckling of the rock structure in the hanging-wall and shear as well as rotational failure by slip and abutments. This, however, is not relevant to this study, but is extensively reviewed and presented by Bandis *et al.* (1981) and Bandis *et al.*(1983)

2.1.2 Support Types and Performance Characteristics

Over the years many support technologies have been developed to support, yield and absorb the energy for different ground conditions in underground mining. It became necessary to define and quantify variables for ground conditions and support characteristics to be able to design effective support systems.

According to Daehnke *et al.* (2001) the critical rock mass parameters that must be considered in evaluations when dealing with areas where ore extraction is carried out are:

- Height of potential fall;
- *Quasi-static* stope closure rates;
- *Dynamic* stope closure rates;
- Compressive hanging wall stresses;
- Discontinuity spacing, orientation and interface properties.

A big challenge in the ground control system design is to design a support system that will retard the closure rate, but not prevent movement of the rock mass. This must be done to ensure that the rock mass can move elastically to relieve the internal stresses and abutments. If movement is prevented the risk that the *Energy Release Rate* (*ERR*) will be manifested through rock bursts and seismic events are greater because of the abutments in the surrounding rock. One of the main purposes of stope support systems is to carry out the function of absorbing the energy that will otherwise be manifested in higher stope closure rates, rock-burst situations and face ejections.

Stope support design criteria rely on data collected from laboratory testing and *in-situ* surveys to predict the performance of stope support systems. This empirical method of collecting data is an expensive and time consuming method and the data must be updated on regular bases. The reason for this is because the primary method of support in current mining methods consists of timber props and timber packs. The general quality of new timber units, in terms of their mechanical properties, are continuously changing and since the performance of supports systems rely exclusively on the material properties of the installed units, this is an important variable to keep track of.

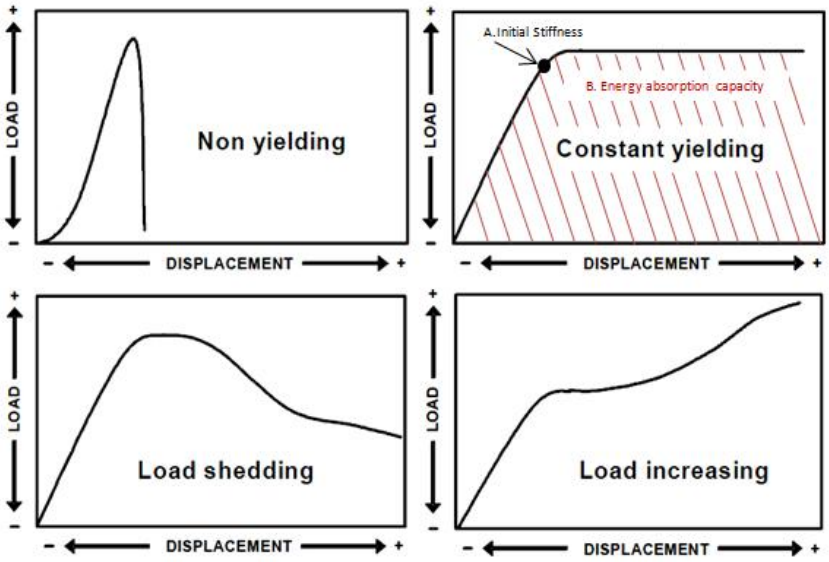

Figure 2. 2: Basic types of load-deformation curves from support units (after Barczak, T.M. 2005)

Support resistance requirements or performance requirements describe the *reaction force* of a support unit for a certain amount of stope convergence (closure). For each support design the *load-deformation curve* (Performance curve) is determined, usually by deriving conservative data from multiple tested units or by empirical data collected from *in-situ* recorded data. The performance of a support unit is determined by three criteria, namely the *energy absorption capacity (Fig. 2.2 B)*, the *initial stiffness (Fig. 2.2 A)* and the *yielding capability*. The *energy absorption capability* of a support unit is quantified by its capacity to absorb energy. This can be determined by calculating the area underneath the *load-deformation* curve. *Initial stiffness* is the load under which the support unit will start to yield. Figure 2.2 illustrates this by the point where the slope of the load-displacement line changes from a predominantly steep linear line to different slopes and shapes. The *yielding capability* is closely related to energy absorption capacity of a support unit and refers to its mode of plastic deformation after yield was initiated.

Different support technologies react different to stope closure conditions as illustrated in Figure 2.2. Brittle types of support, i.e. concrete blocks, tend to have a *non-yielding* characteristic. *Constant yielding* capability, associated with mechanical types of support, is the most desirable type of support since this provides a consistent predictable reaction force. Timber props tend to have a *load shedding* performance while timber packs tend to have a *load increasing* performance.

One of the aims of this study is to determine these performance characteristics of a support design using computerised methods to assist in the design and performance analyses processes of support technologies.

2.1.3 Determination of Stope Support Characteristics

The first step in establishing a systematic approach to the evaluation of support performances is in the testing procedures. One of the most recent procedures for testing support technologies and defining their performance specifications is described by Daehnke *et al.* (2001) where a testing procedure is proposed to evaluate the performance of props. This test procedure places emphasises on repeated tests using the same type of unit of the same size to investigate the variability in the columnar support units' performances and to obtain the statistical distribution of the load versus deformation curves. It entails various laboratory and underground compression tests, and requires twenty-seven support units of the same type, to determine the performance curve of that type and design of support system. The load-deformation curves of these units are determined using the laboratory and underground data that account for different load rate conditions. Even though it is recognized that this is a relative small number of tests to represent an accurate statistical data interpretation, it is deemed adequate to represent the variability in various support types.

Computerised predictive and simulation methods are rarely used to determine the performance characteristics of support technologies. For the purposes of this dissertation, a decision was made to focus on mechanical types of support.

2.1.4 Mechanical Technologies

The purpose of mechanical support designs currently used in the industry is to provide support units with good controllable and predictable yielding capabilities and to simplify the handling and installation procedure. In a study conducted by Daehnke (2001) it is evident that the consistency of props made from uniform material is superior to those of timber based props. The advantage of using materials with well-known and uniform properties, such as metals, over timber is that the performance will remain reasonably consistent for all props of the same design and size.

Mechanical prop technologies can be divided into two main groups: *Hydraulic props* and *Friction props*.

Hydraulic props can be described as single stage hydraulic cylinders. At installation the unit is extended and pre-stressed using pressurised water. It can be pre-stressed to provide an initial active reaction force to the region that is being supported. A check valve at the bottom of the prop maintains the distance setting from the time of installation. A piston in a yield column consists of a yield valve which controls the pressure in the piston. Once the yield pressure is reached, water is released through the control valve into the hollow section of the prop and yielding is initiated. The Omni Prop design is an example of such a hydraulic prop. The performance curve of an Omni Prop produced by *ELBROC Mining Products Pty. Ltd.* is presented in Figure 2.3.

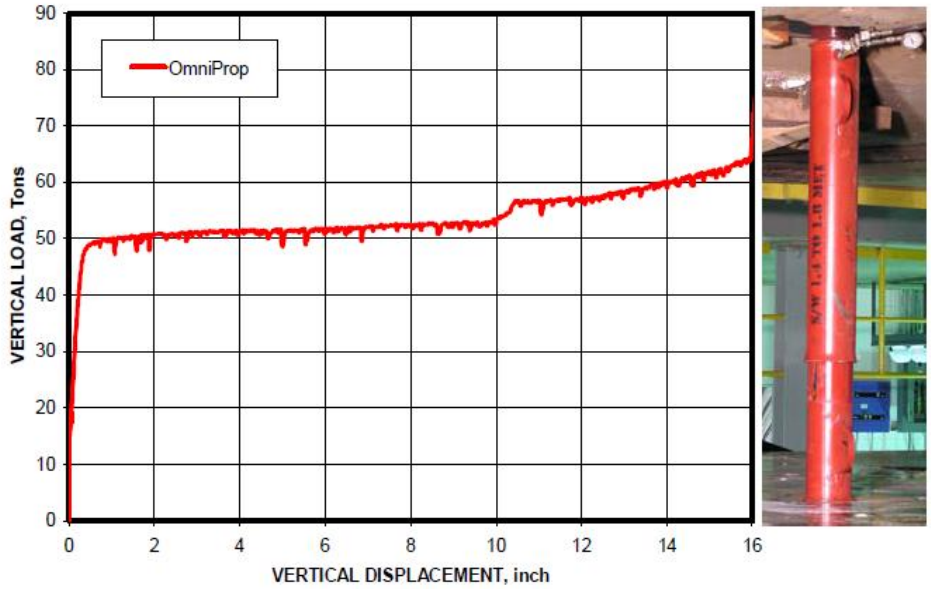

Figure 2.3: Omni Prop performance curve (after Barczak, T.M. 2005)

Friction support technology consists of two main cylinders, an inner and an outer cylinder, that can be extended to different lengths. This technology also uses water pressure to pre-stress the prop and to provide an initial reaction force. Once the initial setting is achieved a collar/deformation wedge is used to lock the unit at a specific length and the water is drained from the support unit. The lower steel tube is then deformed longitudinally as stope convergence occurs. This provides a constant yielding mechanism that is predictable and reliable under different closure rates.

Figure 2.4 presents the performance/*load-deformation* curves for five units of mechanical friction support (rockprop) type tested by *Dynamics Systems Support Pty Ltd*. The units were tested according to the procedure described in Chapter 2.1.3 with an initial loading rate of 30mm/min with an increase to 3m/s dynamic loading rate. From this graph it is clear that the variability of the performance of the mechanical friction support is low, implying predictable behaviour.

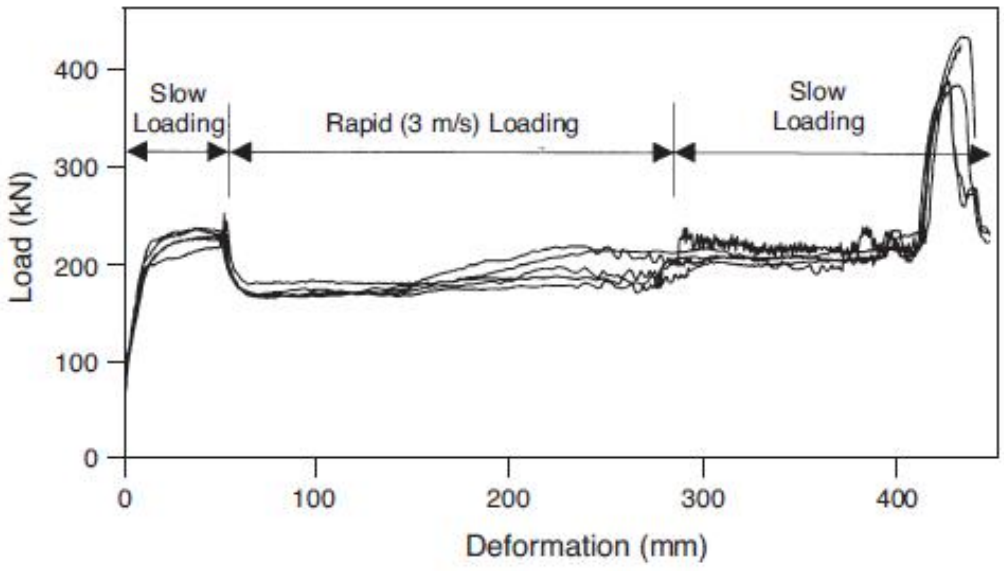

Figure 2.4: Performance curves of five 1.2m rock props from an unspecified manufacturer tested under dynamic testing conditions (after Daehnke, A. et. al. (2001)

2.1. 5 Design Base and Simulation of Support Units

In the case of designs that are made from uniform materials such as metal props and hydraulic props, designs are conducted and analysed using basic fluid and material mechanics of the props subjected to static conditions. These calculations are handy for predicting and designing the initial stiffness and critical buckling loads of a prop, but lack the capability of predicting nonlinear behaviour of materials and thus for *quasi-static* and *dynamic* loading conditions. From these designs, prototype models are made and tested to investigate and observe the behaviour of the prop under *quasi-static* loading conditions. From the observations made during testing, modifications and adjustments are made to the design to change and/or improve the behaviour of the design, followed by another prototype subjected to testing. This process continues until the designers are satisfied with the results.

Computerised simulation systems, which include *FEM* systems, are designed to predict the behaviour and reduce the amount of physical manufacturing and testing of designs in order to speed up the development process and reduce the cost, energy and time associated with *trial and error* design processes. The current study aims to review the application of *FEM* in design and analyses processes of mechanical stope support technologies.

2. 2 FEM Parameters in Stope Support Design

Over recent years software have been developed to have capabilities of solving complex practical engineering and other problems using suitable mathematical models and numerical

methods. These processes and resources have become a valuable instrument in the hands of engineers to predict and estimate characteristics of a system that is defined by mathematical models. This is called numerical simulation. The mathematical models that can be solved in the numerical simulation process are usually a set of equations that express the features of a physical system in terms of variables that describe the system. In *Finite Element Analyses (FEA)* a given domain is defined as a collection of sub domains. This is done because it is easier to represent a complicated function as a collection of simple polynomials.

FEA software is being developed to do numerical simulations for different fields of study. In engineering applications there are software that can simulate structural models as well as fluid, electrical and heat-transfer models. These simulations can even be combined in the modern *FEA* simulation software. There were no examples found in the literature where *FEA* was applied to predict the performance of stope support designs but *FEA* software are commonly used to simulate similar mechanical phenomena. Key concepts in the simulation of the *load-deformation* curve of a stope support unit are: Structural, Buckling, Transient/time-dependant and Non-linear Material behaviour.

In modern software it is possible to do simulations that are defined in one dimension, two dimensions and three dimensions. If the geometry allows it, three-dimensional models can be simplified by defining one or more symmetry planes and even symmetry around an axis can be defined.

Transient-structural analyses systems are programmed for this kind of simulations; it is designed to determine the time-dependent response of a structure as a result of any general time-dependant load. It provides capabilities to control time-step calculations, and in modern *FEA* systems it can be used to simulate linear or non-linear material behaviour. (ANSYS™ 13.0).

With the added capability of simulating transient/time-dependent problems in some *FEA* software, it seems that the performance characteristics of stope support prop designs can be simulated and analysed using these systems.

2. 2.1 Axi-symmetric models

Axi-symmetric simulations are used in situations where the geometry, loading and boundary conditions are symmetric around the vertical or z-axis as shown in Figure 2.5. A further requirement for a model to be considered suitable for axi-symmetric simulations is that the geometry, loading and boundary conditions must be independent of the circumferential or the θ direction as shown in Figure 2.6. If the geometry of a support unit can be reduced to an axi-symmetrical model, it can significantly reduce the solution time and effort of a simulation compared to that of three-dimensional simulations.

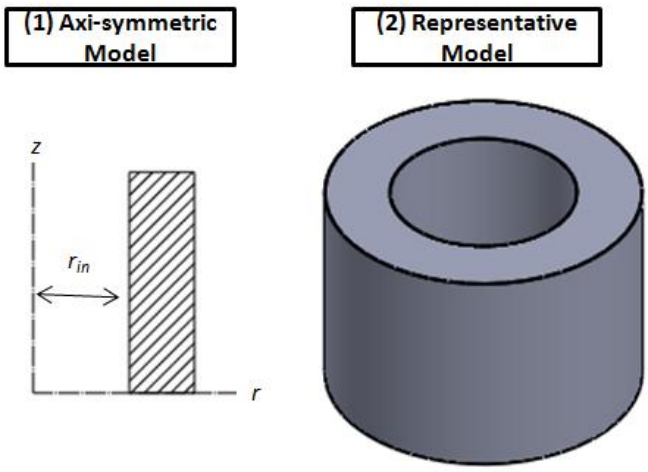

Figure 2.5: Axi-symmetric FE model of a 3-D solid model. (Modified after Mac Donald, B.J. 2011:135)

In such a case where a model can be assumed to be axi-symmetrical, cylindrical coordinates are used to describe the equations and mathematical models governing the physical processes. Plane stress problems (two-dimensional simulation models) only consider stresses that exist in a single principle plane, i.e. in the *x-y* plane. In axi-symmetric problems where a radial displacement exists, circumferential strains that induce stresses in the *r*, θ and *z* direction (where *r*, θ and *z* indicate the radial, circumferential and longitudinal directions) are considered as presented in Figure 2.6. These stresses, σ_r, σ_θ, σ_z, τ_{zr} and τ_{rz} are also presented in Figure 2.6. Logan (2002), Reddy (2006) and Mac Donald (2007) give detailed derivations and descriptions of the stiffness matrix of body and surface force matrices for axi-symmetrical simulations.

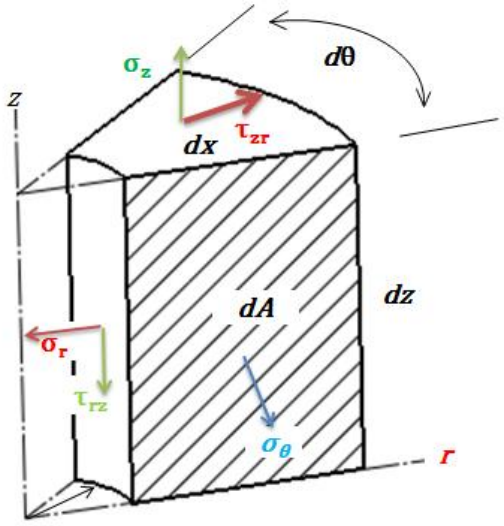

Figure 2.6: Volume element and stresses considered of an axi-symmetric problem. (Modified after Mac Donald, 2007 and Logan, D.L. 2002:71136)

2. 2.2 Three-Dimensional (3D) Stress Analyses

Three-dimensional simulations are often the most intuitive kind of simulation to be done. In many cases however, it is expensive and unnecessary compared to two-dimensional simulations because of the complexity of the analyses setup. It is however useful for three-dimensional bodies that require more precise analyses than is possible through two-dimensional and axi-symmetric analysis and it also provides for a good visual interpretation of the results of the simulation study.

The normal and shear stresses in a three-dimensional infinitesimal element with Cartesian co-ordinates with dimensions *dx*, *dy* and *dz* are presented in Figure 2.7. In this figure the relevant stresses are also shown, normal stresses, σ_x, σ_y and σ_z, are perpendicular to the faces. Shear stresses act in the face planes of the element and are represented by τ_{xy}, τ_{yz} and τ_{zx}. It can be shown from the moment equilibrium of the element that $\tau_{xy} = \tau_{yx}$, $\tau_{yz} = \tau_{zy}$ and $\tau_{zx} = \tau_{zx}$ (Logan, 2002:421) This forms the basis of the calculations during a structural analysis of a three-dimensional simulation.

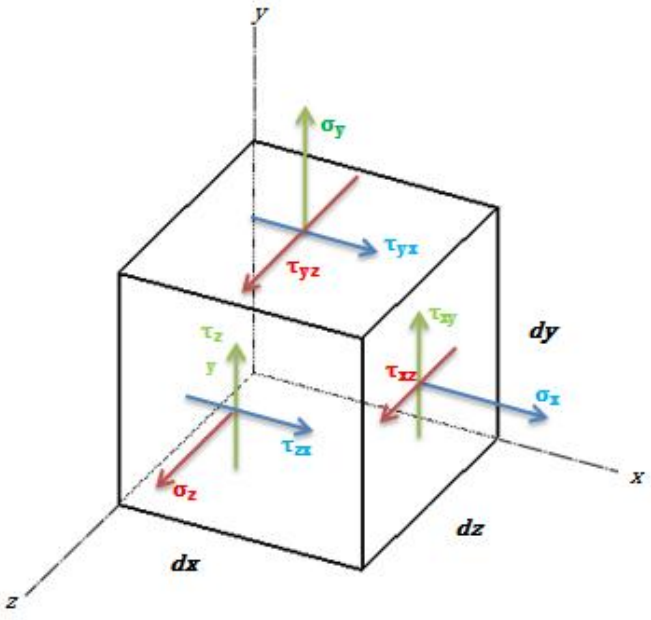

Figure 2.7: Stresses on a tree dimensional element (Modified after Logan, D.L. 2002:422)

All the detail and considerations regarding the strain/displacement function, stress relationships, stiffness matrix and equations and body and surface forces are extensively discussed in Logan (2002), Mac Donald (2007) and Reddy (2006).

2. 2.3 Meshing

An important step in *FEA* is to divide the models that are being simulated into equivalent systems of finite elements with associated nodes. This procedure requires good engineering

judgement and skill because these elements should be small enough to give usable and accurate results and large enough to minimize computational effort. A handy method to obtain these sizes is to conduct mesh independent analyses. According to Logan (2002:320) the smaller the mesh-size – hence more elements in the system – the closer the answer will be to the exact solution. This is illustrated in Figure 2.8 and is important to deal with since it can have a significant effect on the estimated results generated by the simulation. A mesh independent study usually consists of a series of simulations with decreasing mesh sizes and a comparison between the results. From this comparison it can determined in which cases the results are less dependent on the mesh size and an appropriate size can be chosen.

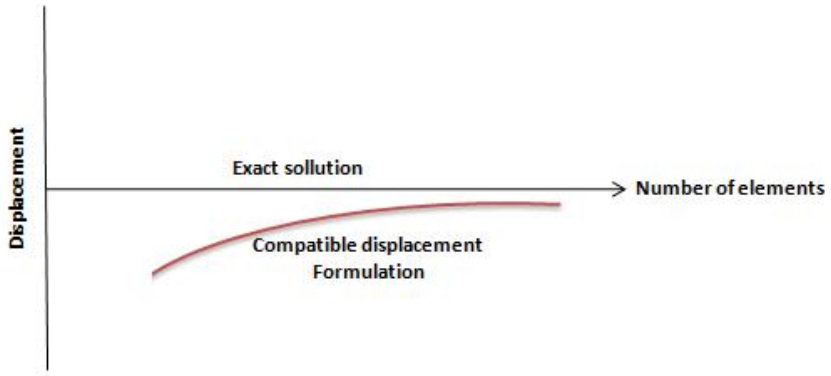

Figure 2.8: Convergence of a FE solution based on the compatible displacement function (Modified after Logan, 2002:71)

The choice of the most appropriate type of element is also one of the major tasks to be carried out by the analyst. For each type of simulation (two-dimensional, three-dimensional etc.) various types of elements can be used and each type of element has its unique computational characteristic.

Even though a two-dimensional surface and elements are used to define an axi-symmetric body, the elements are considered to be three-dimensional in the computational models. This concept is discussed in Chapter 2.2.1. These types of elements are shown in Figure 2.9.

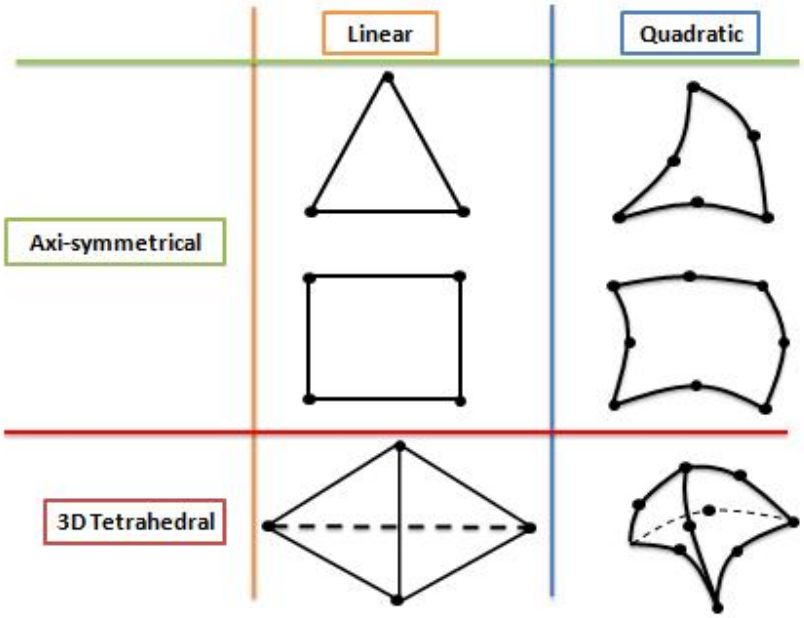

Figure 2.9: Linear Axi-symmetric elements. (Modified after Mac Donald, 2011:121)

The linear quadrilateral element has four nodes where the linear triangular element has three nodes. The tetrahedral element and the hexahedral element are the most common elements when working with three-dimensional models. The linear tetrahedron is a four node solid as presented in Figure 2.9.

Axi-symmetrical, two-dimensional elements and three dimensional elements can be either linear or of higher order. Higher order elements can be developed by adding additional nodes (called mid-side nodes) to the sides of the linear element. With these elements higher-order strain variations can be achieved within each element and convergence to the exact solution can be achieved more accurately using less elements. Higher-order elements can also be advantageous when working with models with curved boundaries. In these cases the shapes of the boundaries can be estimated more accurately with non-linear elements. It should be noted that higher-order elements can increase the computation time in certain cases to such an extent that it is not financially sensible to use them at all. Figure 2.9 presents the difference between two-dimensional linear and quadratic elements and also presents the difference between a linear tetrahedron and a quadratic tetrahedron. It is possible to use elements with an even higher order than that of quadratic elements.

2.2.4 Material Setup and Non-linear Material Models

In normal structural simulations it is assumed that the material behaves in a linear-elastic way (Fig. 2.10). In these simulations a *factor of safety (FOS)* is used to determine the critical areas of the structure or system under investigation. When analyzing and modelling nonlinear material behaviour however, it is necessary to use nonlinear material models.

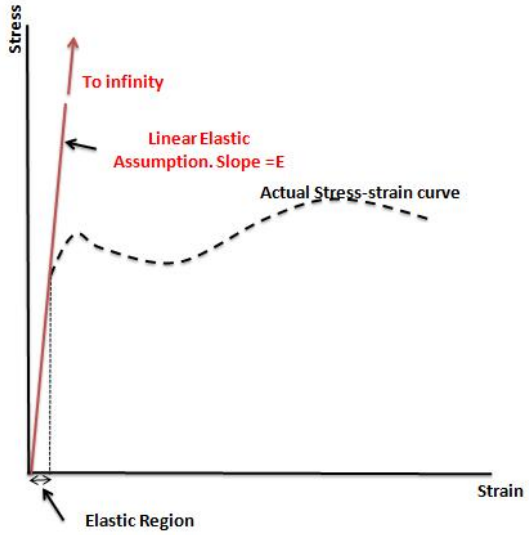

Figure 2.10: Linear Elastic Material model. (Modified after Mac Donald, 2011:163)

The majority of stope support technologies depend on non-linear deformation to generate a reaction force. The nonlinear material models assume nonlinearities in the behaviour of the structure, i.e. yielding, and are derived from the actual *stress-strain curve* of the material. The existing models can be divided into three main groups, namely *bilinear* models, *multi-linear* and *Power Law* models, illustrated in Figure 2.11.

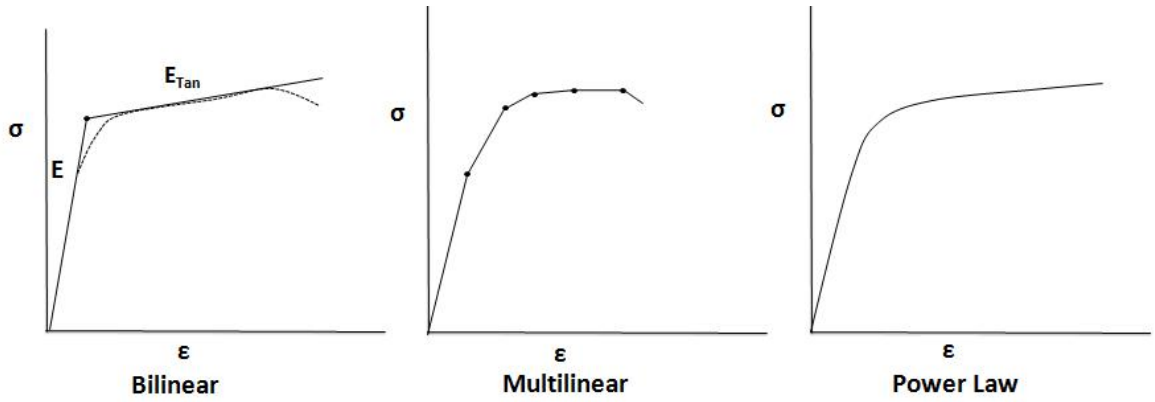

Figure 2.11: Different groups of material models – stress strain behaviours. (Modified after Mac Donald, 2007)

Some of these models are expanded for higher strain rate conditions and high or low temperature conditions etc. To derive such models for a material involve expensive equipment and time consuming experimental processes. Some of the models that are used by simulation software packages include:

- Bilinear Isotropic hardening;
- Multilinear Isotropic hardening;
- Bilinear kinematic hardening;
- Multilinear kinematic hardening;
- Chaboche kinematic hardening;
- Anand Viscoplasticity;
- Johnson-Cook strength;
- Cowper-Symonds Strength;
- Steinberg-Guinan Strength and;
- Zerilli-Armstrong Strength.

Each one of these models has its strengths and limitations, for instance the constitutive models such as the *Johnson-Cook Strength* or the *Zerilli-Armstrong Strength* material behaviour models are preferred for simulations where high strain rates are present. Other analytical models are often used in simulations where lower strain-rates are being simulated.

Bilinear material models

Subsequent to the *Elastic-Perfectly Plastic Model* (*EPPM*), the *bilinear* model is the most fundamental and basic non-linear material model that is used for stress analyses problems. The main difference between the *EPPM* and the *bilinear* model is that the *EPPM* assumes no hardening or softening after yielding.

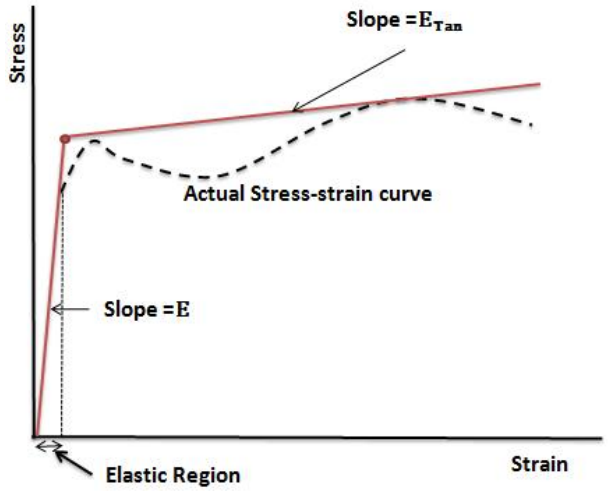

Figure 2.12: Bilinear material model. (Modified after Mac Donald, 2011:177)

The Bilinear hardening model presents two lines in the stress strain curve: One for the elastic behaviour of the material, before yielding is initiated, and the other for the plastic behaviour of the material. This model is illustrated in Figure 2.12 and is derived from a typical *stress-strain* curve for a metallic material.

A straight line is used to estimate the highly curved nonlinear part of the actual stress-strain curve of the metal. The tangent modulus (E_{Tan}) is the slope of the second approximation line. In cases where the stress-strain diagram is available this line is obtained by drawing a tangent to the nonlinear portion. If there is no accurate stress-strain data available, the tangent modulus can be obtained by using the equation:

$$E_{Tan} = \frac{\pm_U - \pm_Y}{£_{fail} - £_{proof}} \qquad (2.4)$$

where: σ_U is the ultimate stress of the material

σ_Y is the yield stress of the material

ε_{fail} is the material failure strain

ε_{proof} is the proof strain (usually assumed to be 0.002) of the material. (Amount of strain that is recovered when the load is released.)

This model is usually used when there is an absence of more accurate data or as a first guess for nonlinear behaviour. Since the tangent modulus does provide the prediction of strain-hardening (since the slope would rarely be zero) it seems appropriate to discuss the hardening laws in the following section.

Hardening Laws

There are two different hardening laws that divide the bilinear model into two forms namely the *bilinear isotropic hardening* and *bilinear kinematic hardening*. The hardening laws are used to describe the way that the yield surface will change with the continuation of yielding, so that the stress state for subsequent yielding can be established. Any stress state inside the yield surface is elastic and outside the yield surface is plastic. The *isotropic hardening* rule states that the yield surface will remain centred about its initial centre line, as the plastic strain develops the surface will expand in size about the initial centre line. The *kinematic hardening* model assumes that the yield surface will change location with developing yielding but will remain the same size. Both these hardening modes are illustrated in Figure 2.13.

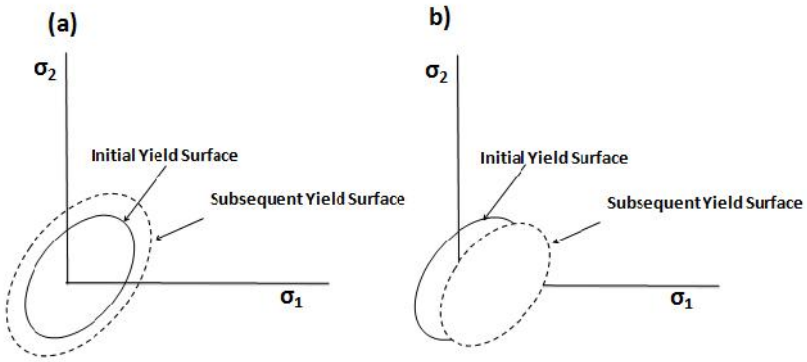

Figure 2.13: (a) Isotropic Hardening law and (b) Kinematic Hardening law. (Modified after Mac Donald, 2011:178)

The *bilinear kinematic hardening model* assumes that the total stress range is equal to twice the yield stress. This is known as "*Bauschinger effect*" and is illustrated in Figure 2.14 (a). The *kinematic hardening model* is more suitable for situations where small strains are experienced in materials that obey the von-Mises yield criterion. The *bilinear Isotropic* hardening is more suitable for applications where large strains are experienced. This model also uses the *von-Mises* yield criterion and assumes that the total stress range is equal to two times the *Ultimate Tensile strength (*UTS*)* (Fig. 2.14 (b)).

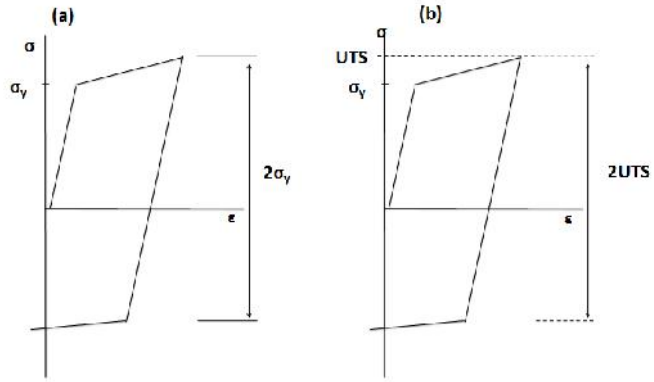

Figure 2.14**: (a) Bilinear kinematic model and (b) Bilinear Isotropic model stress-strain. Modified after (Mac Donald, B.J. 2011:179)**

2. 2.5 Body Interaction

Since surfaces in many of the multi-body physical models, such as the deformation mechanism of a friction prop, are not bonded or permanently joined in any way, but are sliding over each other during operation, the obvious conclusion can be drawn that the contact between these surfaces must be frictional. There is however no way to measure the friction factor and it can only be determined through empirical experimental processes using a mathematical model that defines friction in some way. The *classical Coulomb friction* model is a model that mathematically defines friction between surfaces.

The *basic Coulomb friction* model defines "*sticking*" as the shear stress that two contacting surfaces can carry before sliding relative to each other occurs. It further defines the equivalent shear stress **COHE**, at which sliding on the surface begins as a fraction of the contact pressure ***p*.** The real constant, **TAUMAX** is the maximum contact friction with units of stress. This maximum contact friction is introduced so that sliding will occur when this value is reached regardless of the magnitude of the normal contact pressure. **TAUMAX** (Fig 2.15) is typically used in a situation where contact pressures get large such as bulk metal forming processes. Cohesion is a phenomenon that should be addressed in the friction model. This model defines this as a value, in stress units, that provides sliding resistance with even zero normal pressure and is illustrated in Figure 2.15.

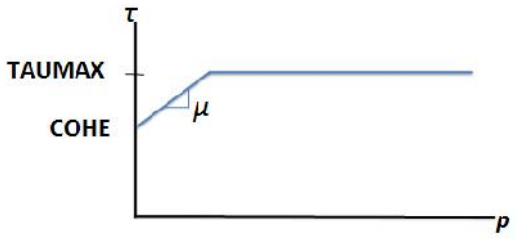

Figure 2.15: Sliding contact resistance (Modified after ANSYS™ 13.0)

The coefficient of friction depends on the relative velocity of the surfaces in contact. The typical trend is that the static coefficient is higher than the dynamic coefficient and the higher the contact velocity, the lower the friction coefficient. The exponential decay friction model that can be used in analyses is given in the following formula:

$$\mu = MU \times (1 + (FACT - 1)\exp(-DC \times V_{rel})) \qquad (2.5)$$

where: μ = coefficient of friction.

MU = Dynamic coefficient of friction.

$FACT$ = Ratio of static to dynamic friction with a default value of 1.

DC = decay coefficient. When DC = 0, the equation is written

$\mu = MU$ for the case of sliding and

$\mu = FACT\ x\ MU$ for the case of sticking.

V_{rel} = Relative slip rate between surfaces.

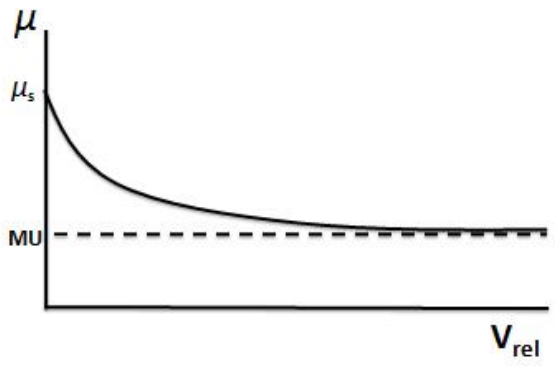

Figure 2.16: Graph of Exponential friction decay, μ vs. relative contact surface velocity (Modified after ANSYS™ 13.0, Guidelines)

Figure 2.16 presents the friction exponential decay curve employed by *ANSYS™* simulation software. Analyses with surface-to-surface contact problems use Contact Algorithms to define the contact between the two surfaces. The following models are typically used:

- Penalty method (or Pure Penalty method);
- Augmented Lagrangian;
- Lagrange multiplier on contact normal penalty on tangent;
- Pure Lagrange multiplier on contact normal and tangent (or normal Lagrange as specified in *ANSYS™*);
- Internal multipoint constraint calculation methods.

The default option in the simulation interface, of the *ANSYS™* simulations software, is set to "*Pure Penalty*". This method uses a contact spring to establish a relationship between two surfaces using the stiffness of the spring which is called the contact stiffness. In simulations where high surface-to-surface contact pressure is experienced and of high importance, it is preferred to use the normal Lagrange method. The normal Lagrange multiplier method enforces zero penetration between contact elements when the contact is closed and zero slip when sticking contact occurs. This method uses chattering control parameters rather than contact stiffness which adds contact traction to the model as additional degrees of freedom. This may increase the computational cost of the simulation because it requires additional iterations to stabilize the contact conditions (*ANSYS™* 13.0).

2. 3 Buckling of columns

Dahenke *et al.* (2001) discusses the relationship between buckling of columns, support height and length of support columns. From this background it is evident that buckling is major cause of failure in underground support props. An aim of this study is to determine the theoretical potential of buckling on the columnar support props. For this reason it was necessary to review the theory of buckling.

The theory of buckling can also be defined as the theory of stability of a slender column. A column subjected to a compressive force can be seen as a system that is stable under loading condition for a force smaller than the *critical load*, and will become unstable when the force is equal to or greater than the *critical load* for that system.

Columns that are subjected to a certain *critical load* may fail by a sudden lateral deflection, also called buckling, rather than failing by *yielding or crushing*. This lateral deflection, if it increases, causes the column to undergo plastic deformation and possibly a catastrophic fracture or collapse. When an investigation is done on a column it is usually initially assumed that the column is an *ideal column*. An *ideal column* is defined to be a column manufactured from a uniform material that remains elastic, is not subjected to a bending moment or lateral force, is subjected to a compressive force along its central longitudinal axis and is weightless and free of residual stresses (Boresi, 2003:423). Some of the methods used to determine the *critical load* for conservative systems include:

- The energy method;
- Snap through method;
- The equilibrium method (leads to the Eigen value problem);
- Imperfection theory and;
- The dynamic method.

These methods are discussed by authors such as Boresi *et al.* (2003) and Hibeler (2005)

2. 3.1 Concepts of buckling

An initially straight column with pinned ends will theoretically fail when it is subjected to a large compressive force, P_{cr}, where P_{cr} exceeds the magnitude of *the critical load* (Hibeler, 2005:673):

$$P_{cr} = \frac{\pi^2 EI}{L^2} \qquad (2.6)$$

where E is the modulus of elasticity, I is the moment of inertia of the cross section area about the axis of bending and L is the length of the pinned-end column presented in Figure 2.17(a). If the compressive load on an ideal pinned-end column exceeds the critical load P_{cr} the column is in an unstable equilibrium state. It may happen that the compressive load exceeds the critical load, following the line *OC* in Figure 2.17(b), and then failure may occur at a load $P \geq P_{cr}$ (Boresi, 2003:424). A more realistic behaviour is shown by the curved dotted line in Figure 2.17(b).

Most columns will in reality be slightly bent and the line of action of force *P* will not be exactly along the central axis of the column and hence perform their function as a beam-column. The stress in the in the column due to the critical load, P_{cr}, is:

$$\sigma_{cr} = \frac{P_{cr}}{A} = \frac{\pi^2 E}{\left(\frac{L}{\rho}\right)^2} \qquad (2.7)$$

where σ_{cr} is the critical stress in the column, L/ρ is the slenderness ratio and A is the cross sectional area of the column (ρ is the radius of gyration $\rho = \sqrt{\frac{I}{A}}$). For the column to remain elastic, σ_{cr} must be lower than the yield strength of the material of the column.

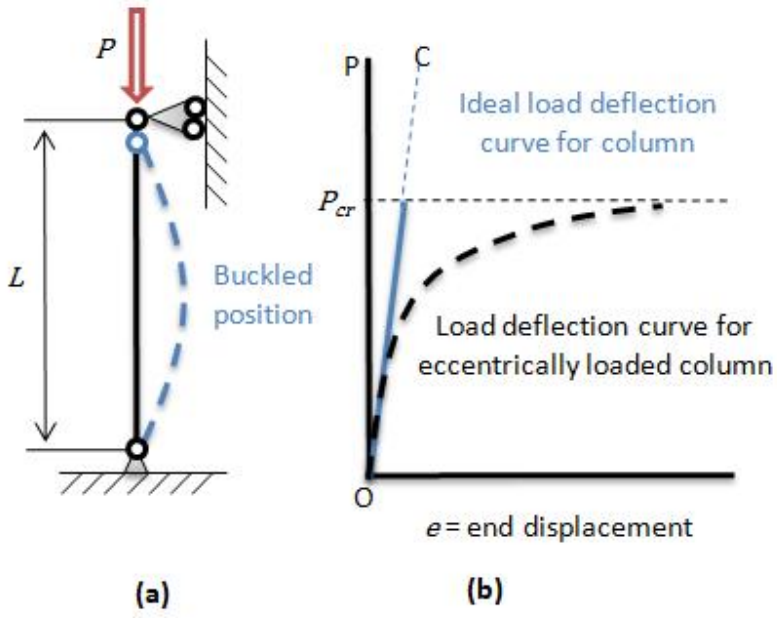

Figure 2.17: (a) Pinned end column and (b) Load-Deflection curve (Modified after Boresi,2003)

According to the Euler formula for columns with pinned ends, a column has more than one critical load where:

$$P_{cr} = \frac{n^2 \pi^2 EI}{L^2} \qquad (2.8)$$

and n is the value of the buckling mode. Columns may buckle in modes for $n > 1$. The buckling load for which a column is the weakest, hence the most conservative choice in buckling analyses, is for $n = 1$. This is also the situation where a minimum critical load is required to buckle the column. Boresi *et al.* (2003) comprehensively discusses higher buckling modes.

The minimum buckling loads for columns with other end conditions than pinned-ends are given by

$$P_{cr} = \frac{\pi^2 EI}{L_{eff}^2} \qquad (2.9)$$

where L_{eff} is the effective length of the column with a specific end condition. The factors that are used to determine L_{eff} for different end conditions are summarised by authors such as Boresi *et al*. (2003) and Hibeler (2005).

The *Euler* formula becomes an unrealistic approach at a slenderness ratio where the critical buckling stability limit is equal to the elastic limit. This is shown in Figure 2.18 at point **A** where the slenderness ratios are plotted against the unit load for illustrative purposes.

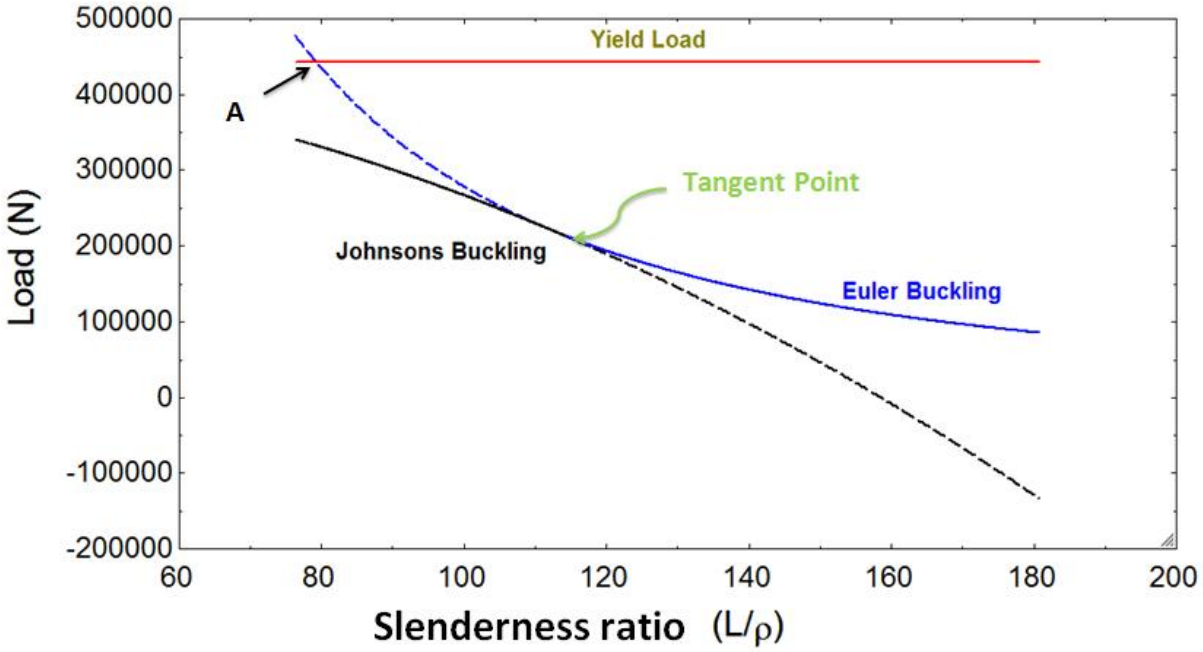

Figure 2.18: Illustrative *Euler and Johnson* buckling curves. (Modified after Juvinall, 2006:211)

To present a more realistic approach for columns with smaller slenderness ratios than is realistic for the *Euler* formula, empirical methods such as the *Johnson's Method* are used. The tangent point between the *Johnson curve* and the *Euler curve* is where the distinction is made between the methods. If the value of slenderness ratio is equal to or more than this tangent point, it is preferred to use the Euler formula. If this value is less than the tangent points it is preferred to use the Johnson formula. This is illustrated in Figure 2.18.

The *Johnson's* formula is:

$$P_{cr} = A\left[\sigma_y - \frac{\sigma_y^2}{4\pi^2 E}\left(\frac{L_{eff}}{\rho}\right)^2\right] \qquad (2.10)$$

where P_{cr} is the *Johnsons* critical load, A is the cross-sectional area of the column σ_y is the yield strength of the material and L_{eff} is the effective length of the column. (Juvinall, R.C. 2006:209-

211). The stress in the column for this critical load can then be calculated using the relationship $\sigma_{cr} = \frac{P_{cr}}{A}$ similar to Equation (2.7).

2. 3.2 Response to impact loading

Deep level mining areas are subjected to seismic events almost on a daily base. This can lead to high velocity impact loading on support systems in stoping areas. To investigate the effect of impact loading (or *dynamic* loading) on a column, a single degree of freedom system (Fig. 2.19) is considered. This is called a *viscously damped spring mass system*. The column and the mass that it is carrying can be seen as a system with a mass m, viscous damping coefficient c, and stiffness or spring constant k.

When this system is subjected to a momentary impulse or impact load it will experiences a certain response in terms of its movement (displacement, velocity and acceleration). The equation of motion can be obtained using Newton's second law for a homogenous system (System with no external force function applied) (Rao, S.S. 2011:261-262):

$$m\ddot{x} + c\dot{x} + k\,x = 0 \qquad (2.11)$$

In this equations x is the displacement response of the mass, $\dot{x}$ is the velocity and $\ddot{x}$ is the acceleration component.

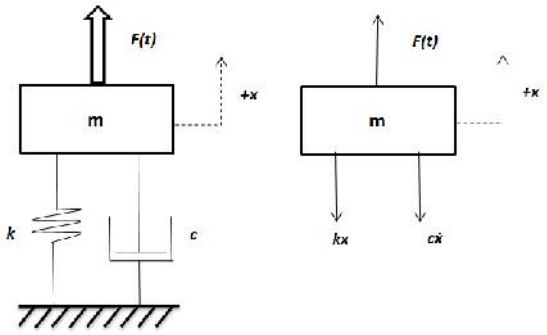

Figure 2.19: Spring-mass-damper system (Modified after Rao, 2011:62)

The *Natural Frequency* of the *viscously damped system* is the frequency of the un-damped system after an initial disturbance. Its value can be determined with:

$$\omega_n = \sqrt{\frac{k}{m}} \qquad (2.12)$$

where ω_n is the natural frequency, k is the stiffness of the system and m is the mass of the system (Rao, S.S. 2011:62). The critical damping constant can be determined with:

$$c_c = 2\sqrt{km} = 2m\omega_n \qquad (2.13)$$

where c_c is the critical damping constant (Rao, S.S. 2011:159-160). The *damping ratio* ζ is the ratio of the damping constant of the system c, to the critical damping constant:

$$\zeta = \frac{c}{c_c} \qquad (2.14)$$

These relations can be used to define the column as a *spring mass damped system* and its response to an impact loading can accordingly be calculated. (Rao, S.S. 2011:62)

The setup discussed above can be used to simulate the response of a support prop that is subjected to dynamic loading conditions.

2.4 Conclusion and Application of literature review

In Chapter 2 a review was done on the processes that are used to design stope support units. It was established that support systems are mainly designed through a trial and error process where units are built, tested and redesigned until the desired performance is achieved. Basic material and fluid mechanics are used in some cases to do preliminary designs. A review to determine the application of *FEM* in the design and analyses processes of stope support revealed that this is a field yet to be explored.

An extensive review was done to establish all the fundamentals that are needed to do a computerised *FEM* analyses. This was preceded by a review on fundamentals and methods to simulate the theoretical potential of buckling on a prop due to different loading conditions.

To apply these fundamentals and determine whether it is feasible to use them in the design and performance analyses of props a case study had to be done. This implies that a specific design and suitable software and computer systems was needed to carry out a comprehensive analysis.

CHAPTER 3 Scope of Study and Modelling Base

Chapter 3 presents the scope of this study and describes the specific support prop design that was chosen to evaluate the suggested method. Finally it describes the software suit that was chosen to do the simulation and obtain results.

3.1 Scope of Study

The scope of this study is to simulate the *load-deformation curve* of a support prop design, using *FEA* computer software. The key result that is of interest is the *performance curve/load-deformation curve* of the unit. It is required that the results obtained be verified in an acceptable manner in order to determine whether computerized simulation is an accurate and sustainable method for this kind of simulation. Furthermore it was concluded from the literature that *buckling of a column* is also applicable to this situation. A decision was therefore made to include a theoretical buckling potential determination of the prop design as part of the impact loading modelling investigation. The Rockprop MK 2 was available as the specimen to execute this study.

3.2 Rockprop MK 2 by Mine Support Products (MSP)

MSP is a company that specializes in the manufacturing of stope support products. The RP 1820E Rockprop MK2, which is manufactured by MSP, was available for this simulation study and this prop proved to be the perfect candidate for the purpose and scope of this study. The manufacturers participated in this study because this simulation study is centred on the fact that testing facilities for *dynamic* loading conditions is currently lacking in South Africa and therefore a simulation of the performance and evaluation of the design and its buckling potential could simplify and reduce the cost associated with the development and improvement of this design and of their extended range of support products.

3.2.1 Description

Rockprop MK 2 is a support technology that uses friction between a collar/deformation wedge and the lower column to generate a reaction force in order to absorb energy with stope closure. It also uses the outward plastic deformation of the lower column as a mechanism to generate the desired reaction force. The development and design of the MK2 was originally carried out by the supplier to provide a compact support unit that is easy to handle and to install with the height of the support unit that can easily be adjusted to suit the specific application and provide maximum stability. The capability of this support prop system to be pre-stressed ensures that a uniform initial support distribution can be achieved with the installation of the system in a stope application which ensures a more uniform distribution of stresses in the hanging wall.

3.2.2 System Components

The Rockprop MK 2 consists of three main components to achieve the desired support characteristics. A schematic of the prop with a maximum length of 2.1 m (that was selected for the current study) is presented in Figure 3.1 accompanied by a Bill of Components in Table 3.1.

The main components are the inner/upper column (2), the outer/lower column (1) and the deformation collar/ deformation wedge (8) (Fig.3.1).

The lower column is manufactured with a dome (5) welded to the bottom, a water inlet socket (7) and the upper end is flared open.

Similar to the lower column, the upper column is manufactured with a dome (6) welded to the top, and a end cap (4) is welded to the bottom to seal off the inner volume of the column and a cup seal (3) is added over the outer diameter to prevent water from escaping from the outer column.

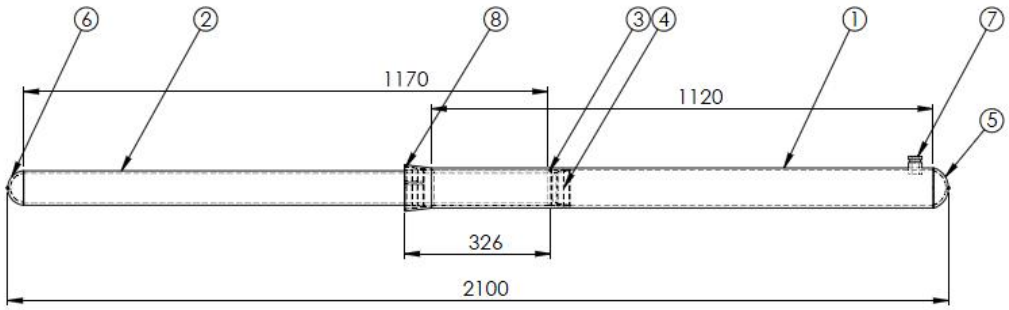

Figure 3.1: Rockprop MK 2 Layout (Source: Manufacturer)

Table 3.1: Component description for Rockprop MK 2

Component Number	Component Description
1	Lower/Outer Column
2	Inner/Outer Column
3	Cup Seal
4	End Cap
5	Lower Dome
6	Upper Dome
7	Water Inlet Socket
8	Deformation Collar/ Deformation wedge

3.2.3 Installation Procedure

The Rockprop unit is transported already assembled but with the inner column retracted to its lowest setting. At the installation location the lower dome is placed in the desired position in a specially designed foot-plate. The function of the domes is to ensure that the compression force is applied as parallel to the support unit as possible to reduce the risk of buckling. In practice this means that a specially designed head plate and a foot plate must be installed above and below the support prop. Water is then pumped into the outer column via the water inlet socket to extend the inner column into position on the hanging wall of the stope. The water pressure is used to pre-stress the unit so that it applies an initial reaction force against stope closure. The cup seal prevents leakage between the two columns and ensures that the pre-stressed load can be achieved at installation and the inner volume of the inner column is sealed off with an end cap to reduce the amount of water needed at installation. When the desired setting of water pressure is achieved the unit is locked in place with the deformation wedge and the water is drained through the water inlet socket. The wedge is forced in to the flared part of the lower column using a special momentum hammer. With this action the collar clamps around the inner column so as to form part of the upper movable assembly.

3.2.3 Mechanical Function and Performance

The compression force that is applied when stope-closure occurs is opposed by the Rockprop. The initial stiffness of the unit is generated by static friction and the resistance that the material of the lower column provides against plastic deformation. Once this is overcome, yielding is initiated and the lower column flares open with the downward movement of the upper section. This mechanism provides the *constant yielding capability* of the friction support. Figure 3.2 presents a *quasi-static* performance curve for a single Rockprop MK2 from a laboratory compression test. From this graph the performance of the support unit for this particular test is evident and in agreement with *constant yielding capability*. The green dotted line indicates the conservative estimated performance curve and the performance parameters, presented in Table 3.2 for illustrative purposes, are then derived from this graph.

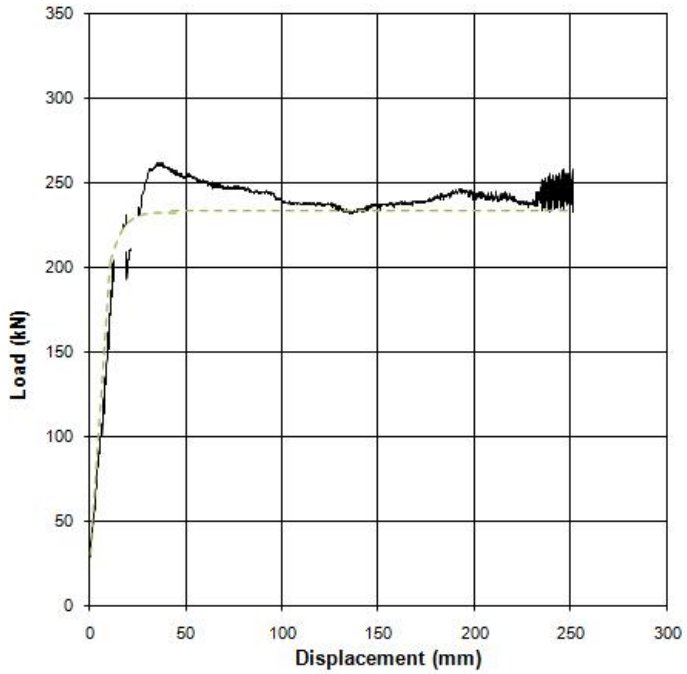

Figure 3.2: Quasi-static Performance curve of a Rockprop MK2 Unit (MSP Laboratory test result)

Table 3.2: Performance Properties of a Rockprop MK

Performance Specification	Value
Initial Stiffness	13 kN/mm
Yield Initiated	210 kN
Yield capability load	232 kN

3.3 Finite Element Analysis system

In order to do a *FEA* simulation of the performance curve, it was necessary to define a computerised model of the Rockprop, its physical properties, boundary conditions and input criteria that is discussed in Chapter 2 for *FEA* applicable the current study.

ANSYS™ offers a number of different analysis options for the simulation of structural, fluid, electric and heat transfer problems and these options can be combined to simulate coupled effects when required for a particular problem. The current study deals with a structural problem where transient effects and non-linear material behaviour are key issues. The transient-structural analysis available in *ANSYS™* are designed for these kinds of simulations and it can be used to determine the response of a structure subjected to general time-dependant loads. It provides automated time step controls and it can be used to simulate linear or non-linear material behaviour. Types of non-linearities that can be modelled with *ANSYS™* include large deformations, plasticity, contact and hyper-elasticity.

ANSYS™ is a software suit that provides a platform for all of the requirements set in this study and is trusted and widely used in the industry. For these reasons *ANSYS™* was chosen to carry out the simulation study.

CHAPTER 4 Simulation Study

Chapter 4 presents the process that was followed to simulate the performance curve of the Rockprop MK 2. Processes that were followed to simplify the models to computerized simulation models are explained in detail along with the general assumptions that was made and assumptions regarding boundary conditions. A detailed overview of the simulation setup is presented with regards to meshing, material model setup and body interactions. The results of the simulations are presented and a comparison is made between the results of the 3D simulation and the axi-symmetric simulation.

4.1 Simulation Setup: Three-Dimensional Simulation

The current study aimed to simulate the *reaction force* generated by the support unit for the vertical displacement of the upper section at a constant velocity to obtain the *load-deformation curve*. The reaction force is generated with (a) the friction force between the interacting surfaces of the deformation wedge and the lower column, and (b) the resistance that the material of the outer column provides to deformation.

4.1.1 Simplification of Design

It was decided to replace the whole upper section and the deformation wedge with only a rigid cone (Fig. 4.1). This was done to simplify the geometry for the simulation process and to cut down on simulation-time. The lower section was replaced with a column with an inner diameter and thickness of the outer column and a length of 350 mm that provided for the rigid solid cone. The testing procedure requires deformation over 250 mm but an extra 100 mm was added to the simulation model to provide for final deformation effects that may be present or that may occur during the simulated deformation. The design model and the simplified 3D model that was used for simulation, generated with the use of *SolidWorks™ 2011* and imported into the *ANSYS™* are compared in Figure 4.1 (a) and (b).

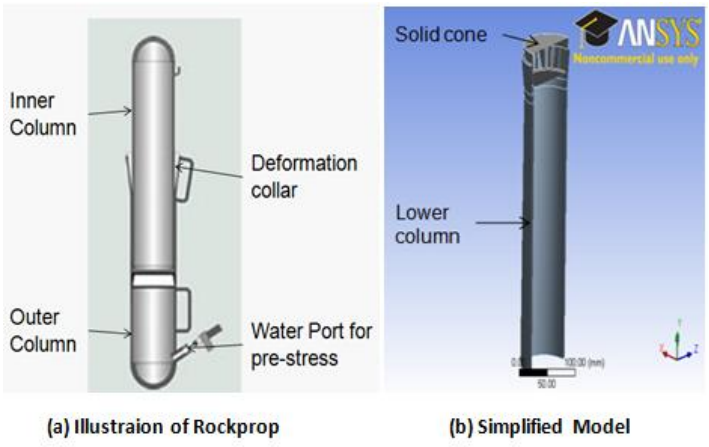

Figure 4.1: Simplified Rockprop Model

4. 1.2 Meshing

It was decided to divide the three-dimensional model into tetrahedral elements as described in Chapter 2.2.3. The tetrahedral element and the hexahedral element are the most common elements when working with 3D models. Normally in a model with the symmetry of the model under investigation it is preferred that hexahedral elements be used as this will ensure a more even and uniform distribution of the stresses and strains experienced by the body. In this case however, the key interests were the reaction force and the global effect of loading and less detail required regarding local stresses and strains. Compared to hexahedral elements, tetrahedral elements also reduce the amount of elements needed to simulate the full 3D model and thus, reduce the calculation time.

4.1.3 Boundary Conditions

The model that is under investigation provides constraints that are adequate to define the mathematical boundary conditions. A fixed support was added to the bottom of the lower column (Fig. 4.2) as the primary boundary condition. This limits the movement of the bottom of the column in the *x*-direction and *y*-direction and, in the three dimensional model, the *z*-direction, albeit the radial direction was not restricted. This constraint eliminates any possibility of movement of the system in the *x*- and *z*-directions and ensures that the desired effect of the radial deformation of the column is simulated. The deformation cone/wedge was free to move vertically downwards (i.e. in the negative *x*-direction), at a specified constant velocity.

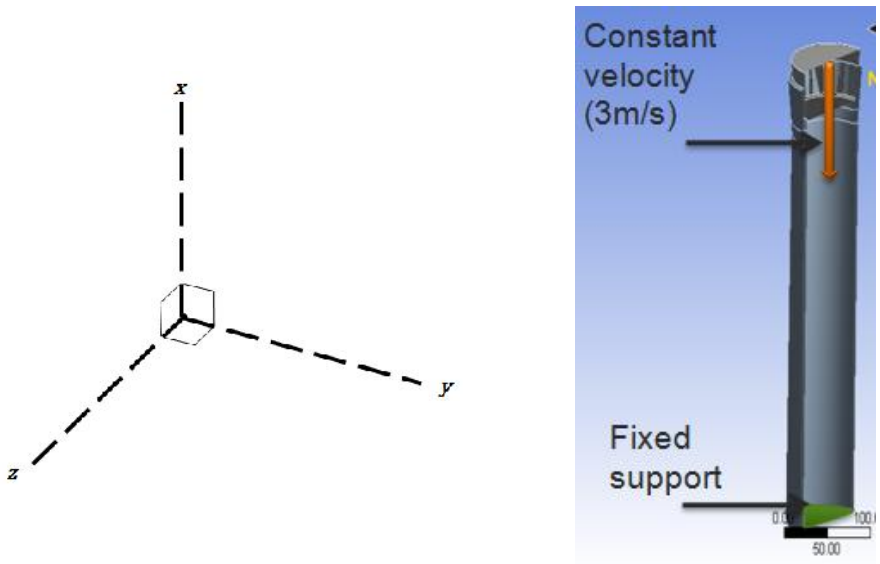

Figure 4.2: Boundary conditions for simulation

4. 1.4 Material Setup

A *bilinear isotropic hardening* model (Chapter 2.2.4) was chosen for this study. The data from laboratory tests, conducted by *MSP,* and presented in Table 4.1 were used to calculate the *tangent modulus* according to the bilinear isotropic hardening model for AISI 1010 steel. Appendix A presents the calculations that were carried out to determine this value.

Table 4.1: 1010 Steel Properties used for simulation of lower column

Description	Symbol	Value	
Yield Strength	σ_y	299	MPa
Ultimate Tensile Strength	σ_u	409	MPa
Elongation	El	43	%
Modulus of Elasticity	E	200	GPa
Tangent Modulus	E_{tan}	2682	MPa

Parameters, such as density and the poisson's ratio, were assumed to be the same as that of structural steel which forms part of the *ANSYS™* database.

For the *quasi-static* simulations, which were compared to actual laboratory data, the bilinear isotropic hardening model was set up for AISI 1010 steel to ensure accurate comparison. With the geometry, meshing, boundary conditions and material properties defined it was important to also evaluate possible interaction between the different bodies.

4. 1.5 Body Interactions

Since the surfaces in these multi body physical models are not bonded or joined in any way, but are sliding over each other during operation, the obvious conclusion can be drawn that the contact must be frictional, or at least frictionless. The friction model that was chosen for this simulation is the *Coulomb-friction model* and the *Normal Lagrange multiplier* was chosen as a contact algorithm because of the high contact pressure that was expected to be present. The theory of these is discussed in Chapter 2.2.5.

4.2 Results: Three-dimensional Study

Simulations were conducted using a *HP 800 Workstation*, with two *Intel Xeon 2.66 GHz Processors and 48 GB RAM*. Problems involving frictional contacting between two surfaces' unsymmetrical stiffness's were encountered in this simulation and gave rise to excessive convergence time.

ANSYS™ uses a symmetrisation algorithm by which most frictional problems is solved using *symmetric* solver systems to simplify the calculations and reduce the calculation time. In the current study this proved to create problems with convergence. To overcome these problems with convergence, it was decided to choose the *unsymmetrical* solution option provided (*ANSYS™*) for the friction model to improve convergence capabilities.

Figure 4.3 presents a section view of the 3D model that was used to do the 3D simulation in *ANSYS™* using *transient structural analyses*. The model setup and boundary conditions were defined as discussed in Chapter 4.1 and a vertical downward velocity of 3 m/s was specified for the deformation cone. This value is based on the standard value for dynamic conditions as defined in Chapter 2.1 for this industry. Because of the fact that the friction factor is an unknown at this stage, the simulation was carried out for various friction factors to investigate the effect of friction on the performance of the prop.

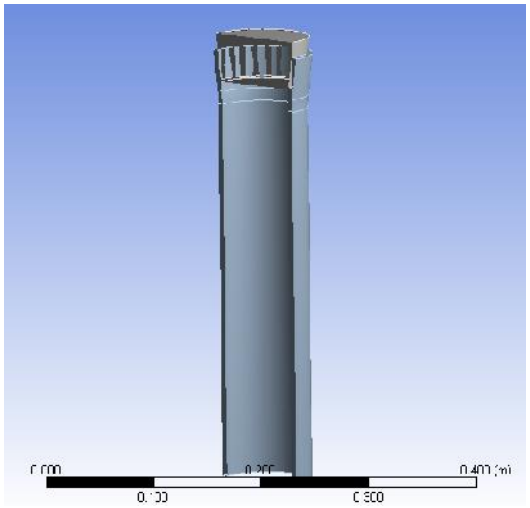

Figure 4.3: Section of Tree-dimensional model

Figure 4.4 presents the *Force-Time* graph and deformed model obtained as a result of the simulation. For the purposes of this study it was required that a *Force/load-deformation curve* be obtained. To do this, the time dependant results were exported and the desired curves were generated using *MATLAB™*. To reduce the distortedness of this graph without lengthy and complex alterations to the convergence criterion, it was decided to filter the results using average- and mean-filtering processes in the *MATLAB™* model.

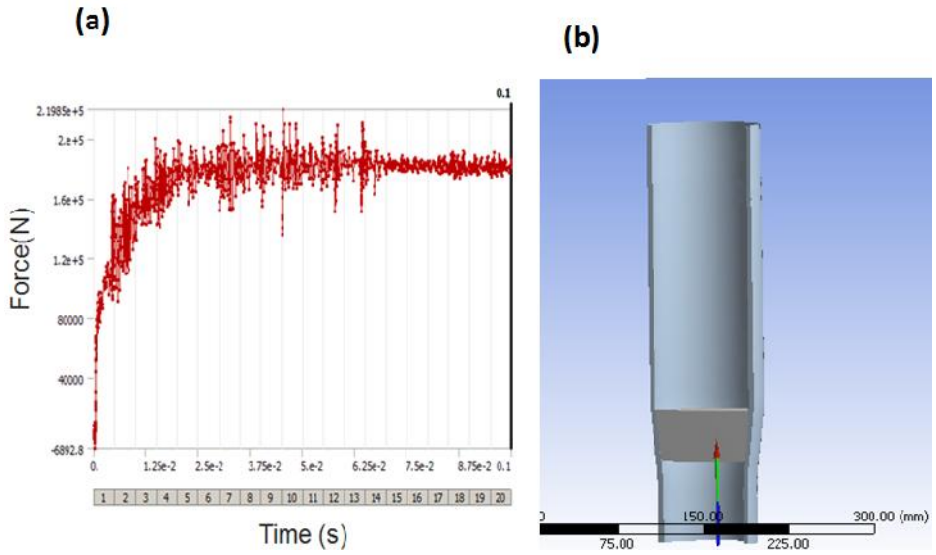

Figure 4.4: (a) Force-Time graph and (b) deformed body from an *ANSYS*™ simulation

Figure 4.5 presents the processed results (*load-deformation curves*) obtained from the 3D simulation model under dynamic loading conditions for different friction factors. These simulations each took between 6.5 and 13.3 hours to complete.

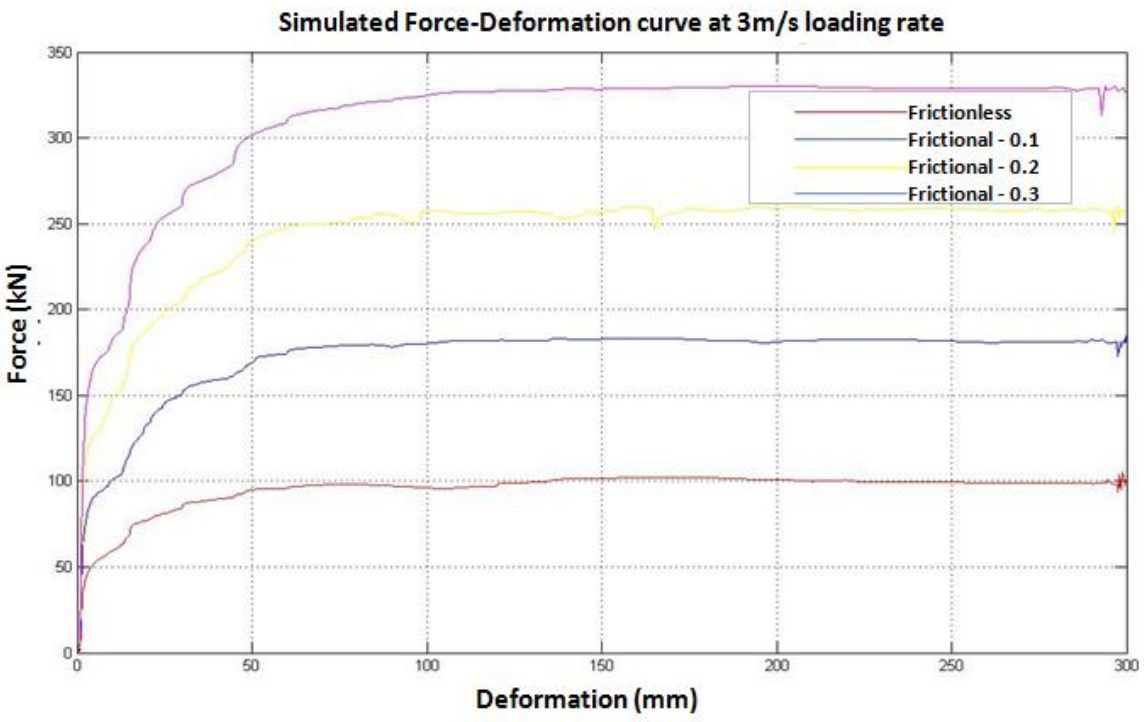

Figure 4.5: Simulated Force-Deformation curve at 3m/s loading rate for different friction factors

From these results it is clear that the trend of the simulated performance curves resemble the trend of performance curves obtained from laboratory testing of models different to the Rockprop MK 2 (Fig. 2.4), and the required curve for a constant yielding mechanism under dynamic conditions (Chapter 2.1.2)

4.3 Simulation Setup: Axi-symmetric Simulation

To validate the results obtained from the three-dimensional simulation it was decided to do an axi-symmetric 2D simulation. This validation study required that numerous simulations be carried out to study the effect of the mesh-size and different parameters on the results obtained in this manner.

Figure 4.6 presents the two dimensional model that was used to do the axi-symmetric simulations. Boundary condition and constraints were defined similar to those of the three-dimensional study, since it was required to compare the results of the different kinds of simulations to validate their accuracy and integrity. The fixed surface defined in the 3D model, for a boundary condition, was replaced with a fixed line (Fig. 4.6) and the 3D deformation cone was replaced with a 2D-surface body (3m/s downward velocity).

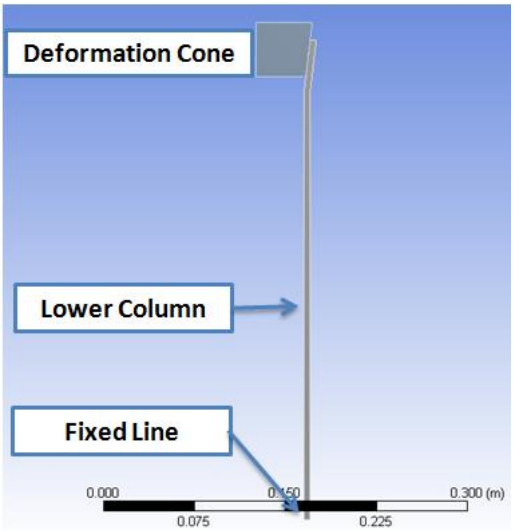

Figure 4.6: Axi-symmetric model used for simulations

4.3.1 Mesh-independent Study

According to standard practice there should be at least three layers of mesh through the thickness of a thin shell when doing an axi-symmetric simulation (Hindley, 2011). For the current study that meant a mesh-size of 1.667 mm for the 5mm thick shell that represents the outer column. To evaluate whether this assumption can be trusted for the current study a mesh-independent study was carried out. With the lack of proper data regarding the friction factor between the contacting surfaces it was decided that a frictionless contact will simplify

the simulation for the purposes of the mesh-independent analysis. The mesh-size was varied between 5mm and 1.667 mm to investigate the dependence of the results on the size of the mesh. The biggest and smallest of these are compared in Figure 4.7 (a) and (b) to illustrate the difference in meshing densities.

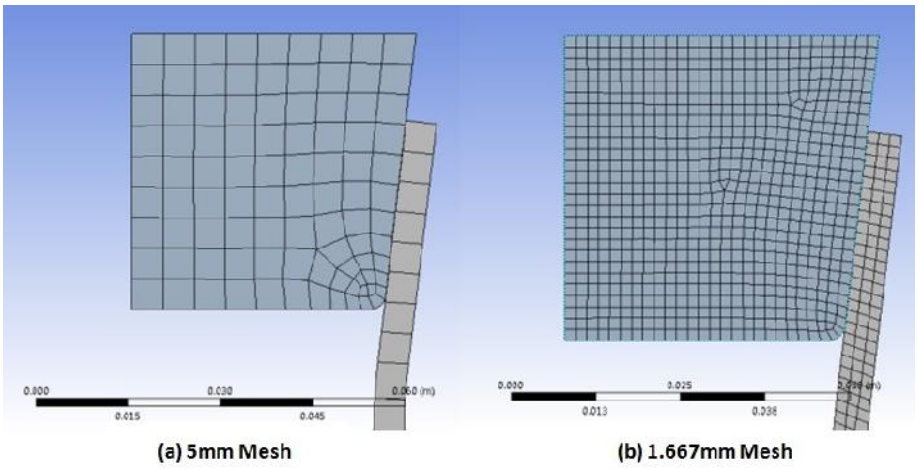

Figure 4.7: Comparison between mesh sizes

ANSYS™ provides useful options for tracking and reviewing the results, such as stresses and strains, deformation, reaction force etc. of a simulation. The results relevant to the current project, to define the performance curve of a prop, are the reaction force measured at the bottom of the outer column, plotted over the vertical displacement of the deformation curve. These results are however presented separately over time (Fig. 4.4) as a result of the structure of the *ANSYS™* algorithms. The same process as discussed in Chapter 4.2 was used to process the data into the desired curves (The filtering process was not required for the axi-symmetric simulations because of the good convergence that was achieved). Figure 4.8 presents the results for the mesh-independent study.

From the results it is evident that the simulated performance curve of the friction prop for this study is almost totally independent of the sizes of mesh that was investigated in this study. It was decided to stay compliant to expert suggestion for the remaining simulations, which means a mesh size of 1.667 mm was used. This was also chosen because of the acceptable solution time for a simulation with this size of mesh.

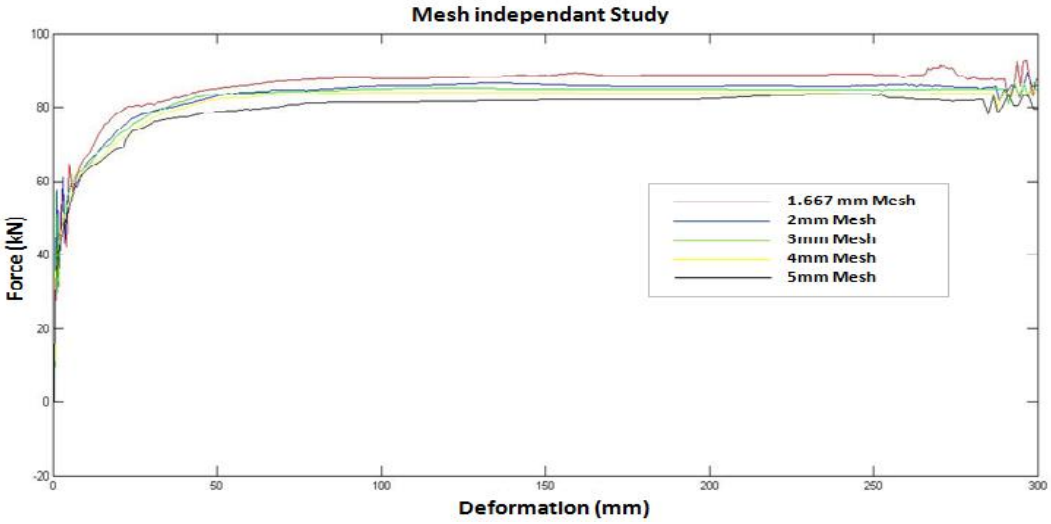

Figure 4.8: Comparison for Mesh-independent study

4.3.2 Three-dimensional simulation and Axi-symmetric simulation- A Comparison of Results

The comparison between the results of the series of axi-symmetric simulations and the results of their equivalent 3D simulations are presented in Figure 4.9.

The trends obtained indicate that there is good correlation between the axi-symmetric and 3D simulations. The different solution times are summarized in Table 4.2 which confirms that axi-symmetric simulations are more economical by some margin.

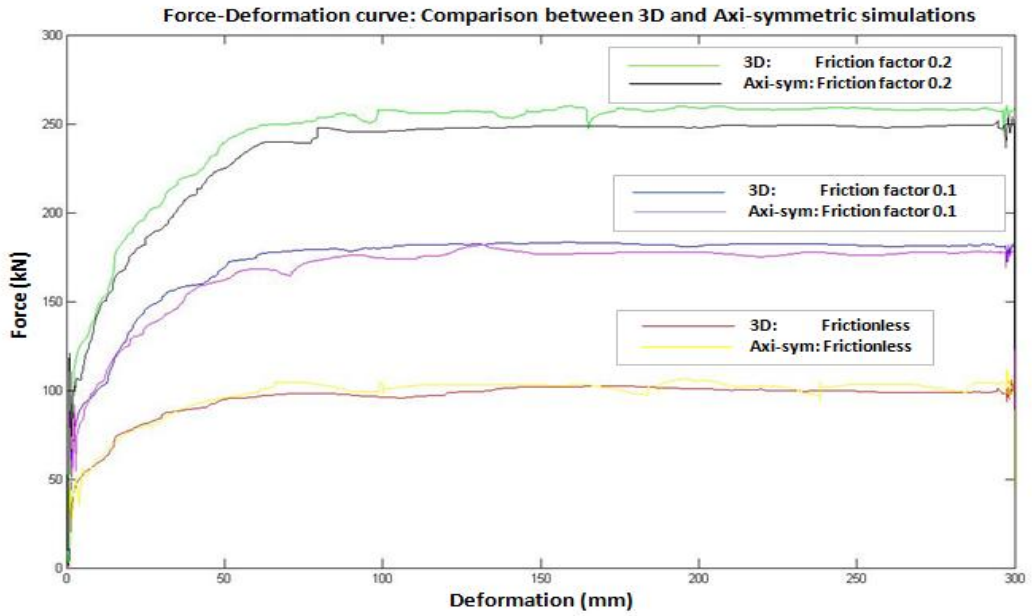

Figure 4.9: Axi-symmetric vs. 3D - Comparison between different Friction factors

Table 4.2: Comparison between solution times of 3D and Axi-symmetric simulations

	Solving Time (seconds)	
Friction Factor	**Three-dimensional**	**Axi-symmetric**
Frictionless	47833	11011
0.1	23096	4287
0.2	33921	5758

4.4 Quasi-static Simulation - Validation of Simulation procedure

The scope of this study required that an acceptable means is used to validate the simulation procedure in terms of a comparison with physically measured data. This could not be done with the simulation of dynamic conditions because of lack of testing facilities that could induce a displacement of 3 m/s. Accordingly it was decided to conduct simulations under *quasi-static* conditions, and compare the results from the simulations with results from tests that were carried out on this specific design (Rockprop MK2) under *quasi-static* conditions.

To obtain the support specification of a prop design, for the use in stope support system design by rock engineers, the design should be analyzed and the manufactured product tested according to the procedure as discussed in Chapter 2.1.3. This section provides performance curves of four Rockprop MK 2 units, with a maximum setting of 2.1m, tested under *quasi-static* loading conditions according to the accepted laboratory testing procedure that can be compared with results from quasi static simulations.

Destruction in comparison tests was done in a laboratory using an 8896 kN (1000 ton) Mohr & Federhaff compression machine. The Rocprops were extended to their maximum height using a hydraulic pump installed between the upper and lower platens of the 8896 kN Mohr & Federhaff compression testing machine. A preload of 200kN was applied to each specimen using the hydraulic pump followed by a gradually increasing compressive load until a displacement of 250mm, or complete destruction was obtained. Figure 4.10 (a), (b), (c) and (d) presents the results from four of these destruction tests. The captions present the serial number for the specific tests that were carried out by MSP.

From the results in Figure 4.10 it is clear that the Rockprop MK 2 units achieve acceptable performance consistency with good comparable performance values under *quasi-static* testing conditions. From the results obtained from simulation studies in Chapter 4.2 and 4.3, and the test results presented in Figure 4.10, it was concluded that the constant yielding mechanism is achieved before a vertical displacement of 100mm is reached and it was reasoned that the simulation can be done up to the 100mm vertical deformation, and that *constant yielding* can be assumed from that point onwards. Figure 4.10 presents the test results compared to the simulated results for different friction factors.

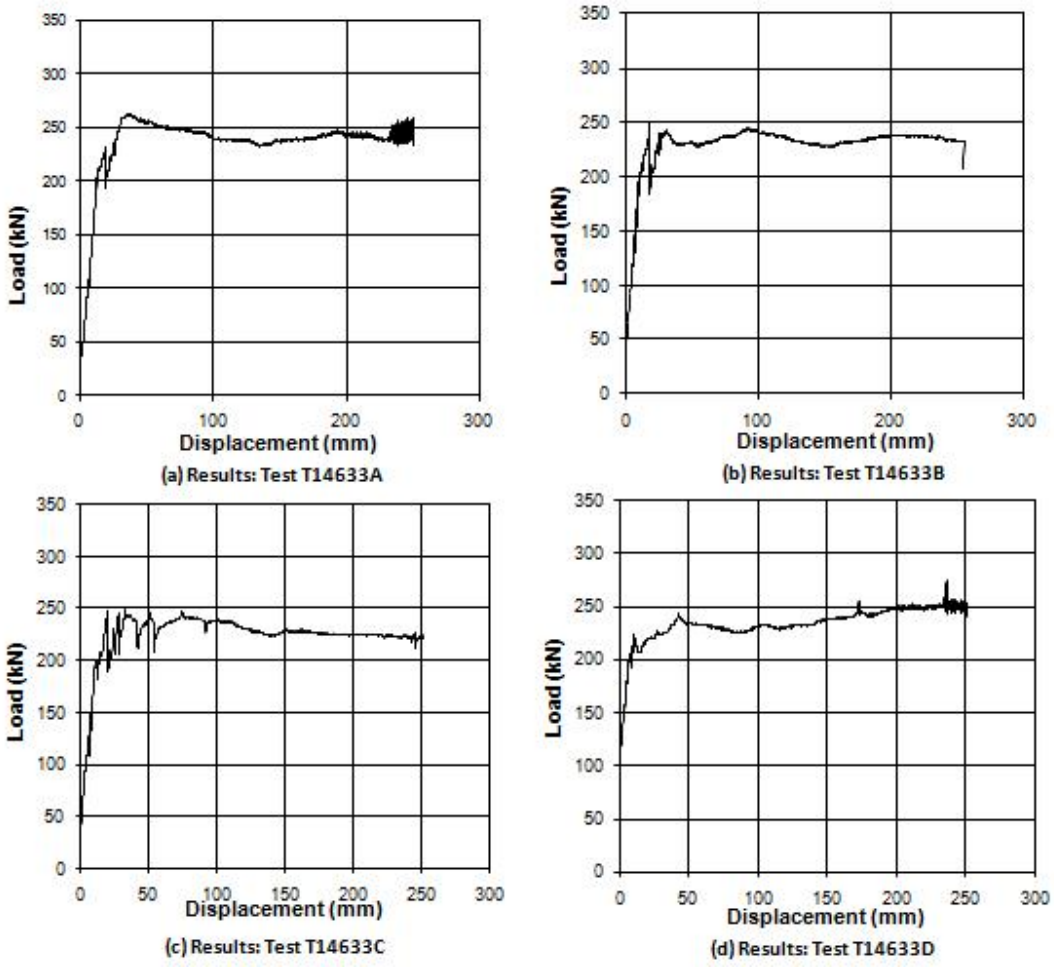

Figure 4.10: Load-Deformation curves from destruction tests done on Rockprop MK2 Units (Manufacturer)

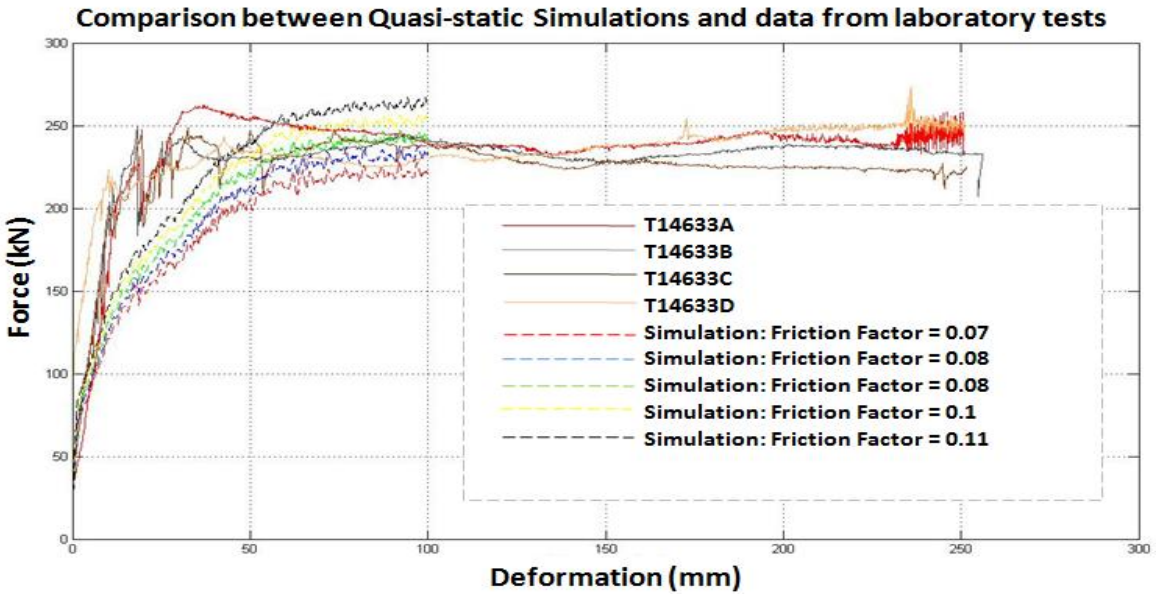

Figure4.11: Comparison between Quasi-static simulations and data from laboratory destruction tests

From the graph (Fig. 4.11), it is evident that the actual friction factor for the units tested varies between 0.07 and 0.1 for the *Coulomb Friction Model* (Dynamic friction coefficient). When comparing the trends of the simulated curves to those of the actual performance curves, it is evident that the initial behaviour differs with regards to the yield point. These differences can be attributed to the lack of the simulation model to consider a *static friction* and the transition from the *static friction* factor to the *dynamic friction* factor as discussed in Chapter 2.3.5. It is however beyond the scope of this study to include static friction in the simulation. This model only considers a constant friction factor through the whole simulation which is defined by the user.

4.5 Conclusion of simulation study

The results achieved in this simulation study, with the assumptions made regarding friction and material behaviour, are considered to be good and conservative representations of the expected actual performance curves for the prop under investigation. It is however noticed that there should be additional attention given to the value of the dynamic friction factor used and to include a static friction factor into simulations to simulate the conditions below the yield point of the performance curve. Furthermore, the material stiffness is possibly affected due to the higher strain rate induced on the system (Johnson *et al.,* 1983); this is not included in the simulations.

This concludes aim of the study in terms of simulating the performance curve of a support prop. The analysis of the theoretical potential of buckling is presented in Chapter 5.

CHAPTER 5 Buckling Study

When dealing with slender columnar members it is crucial to investigate the potential of buckling and stability. Based on the emphasis that is placed on the potential buckling of support props due to the loading conditions in stopes, a theoretical analysis was done to analyze the buckling potential and response of the prop under investigation. The methodology and results of the investigation are presented in this chapter for *static* loading conditions to provide a baseline reference for *dynamic* loading condition that follows.

5.1 Static Buckling of Rockprop MK2 Support Prop Design

As a first step in the determination of the buckling potential and the critical buckling load of the prop under discussion, a static buckling analysis was undertaken.

To ease the buckling analysis it was decided to simplify the design of the MK2 prop for the purposes of modelling and calculations by eliminating complex geometries that do not fulfil a fundamental function in the buckling stability of the column. This action included removal of the domes, the flared part of the lower column, the water inlet socket and the deformation wedge. To eliminate the potential of axial compression of the upper column into the lower column that would normally occur, and to rather enforce potential buckling under load, a further simplification was applied by assuming that the two columns are bonded at the overlapping section (Fig. 5.1) instead of being joined by the deformation wedge.

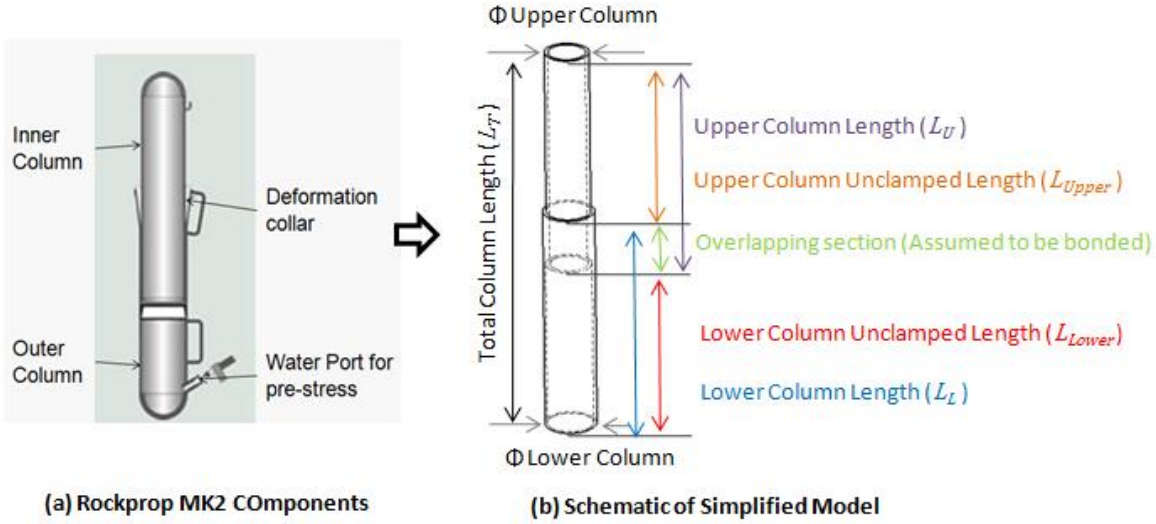

Figure 5.1: Schematic illustrating (a) the components of the Rockrop and (b) a schematic of the simplified model.

The analysis included a computerized simulation and calculations based on standard buckling theory where the simulation and calculations were carried out based on the following assumptions:

- Columns were assumed to be ideal (Chapter 2.3) unless specified to deviate from the conditions of an ideal column
- Because of the highly unpredictable surface mating conditions in underground installations a *clamped-free* and *clamped-simple support* configuration (Fig. 5.2 (a*) and (b))* occur.

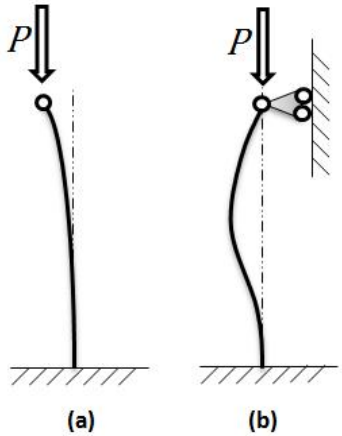

***Figure 5.2: (*a) *Clamped-Free* configuration (b) *Clamped-Simple support* configuration**

A 3D CAD model (Fig. 5.1(b)) was used in a preliminary study using *SolidWorks™ buckling analysis* option for both *clamped-free* and *clamped-simple support* configurations (Fig. 5.2). The engineering properties and geometries used for the modelling and simulation of the bonded column are presented in Table 5.1.

Table 5.1: Engineering and Geometric Properties of Upper and Lower Columns of MK2 RockProp

Description	**Lower Column**		**Upper Column**	
LengthG	1120	(mm)	1170	(mm)
Overlapping section	326			(mm)
Outer Diameter	88.9	(mm)	76.2	(mm)
Wall Thickness	5	(mm)	6	(mm)
Material	SAE 1010		S335	
Young's Modulus	200	(GPa)	213	(GPa)
Yield Strength	285	(MPa)	335	(MPa)

∗ Bonded Lower and Upper column with total column length of L_T (Fig.5.1).

Figure 5.3 presents the deformed shapes obtained from the simulations and tend to show that although the resulting shape for both *clamped-free* and *clamped-simple support* configurations

conform to the expected theoretical shapes under such conditions, the maximum horizontal displacements is of the order of 8.14 mm at a load of 1.6 MN and 1.22 mm at a critical load of 1.12 MN respectively. The *critical loads* obtained in this simulation however causes stresses about 4 times above the *yield strength* of the materials in the lower and upper columns, and therefore unacceptable and inaccurate.

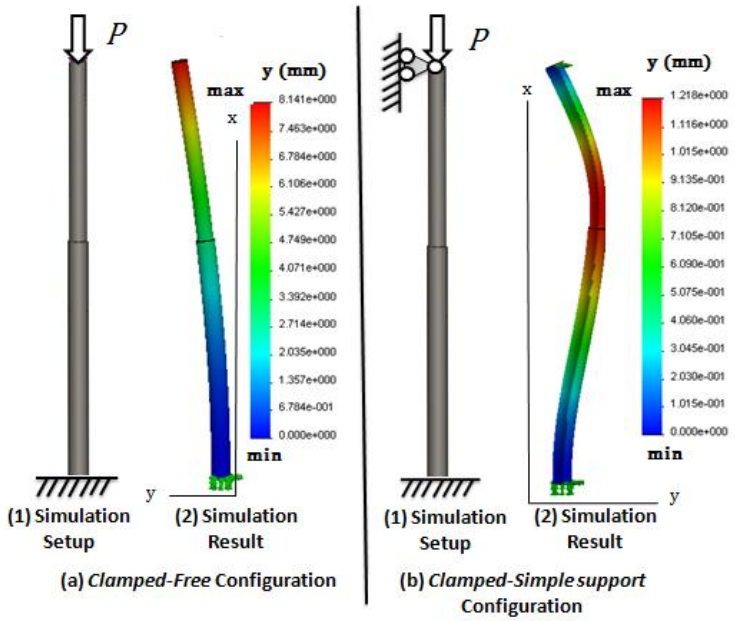

Figure 5.3: Preliminary Buckling simulation Results

In an effort to obtain more reliable values for the vertical loads P, that would induce yielding in the material of the bonded system due to buckling, a *FEM* simulation for both configurations under discussion, was consequently conducted using *ANSYS™ FEA.*

To carry out these simulations with *ANSYS™*, it was required to model columns with pre-induced shapes similar to the theoretical buckled shapes of Figure 5.3. For the purposes of the simulation the required induced imperfect shape for each configuration was obtained by evaluating the shape function (Boresi, 2003):

$$y(l) = a \sin\frac{\pi l}{L_{eff}} \qquad (5.1)$$

where l is the coordinate along the column length and a the amplitude of the function and by setting $L_{eff} = 2L_T$ and $L_{eff} = 0.7L_T$ for the *Clamped-free* and the *Clamped-Simple* support situations respectively (Boresi, 2003:439).

The deviation y (Fig. 5.4) from the ideal column axis was set to 1% of the diameter of the lower column as suggested by the guidelines provided in the *ANSYS™* User Manual section for proper

buckling analyses. This value was used as the axis along which a 3D CAD model was extruded that was imported into *ANSYS™* for the purposes of the buckling analysis.

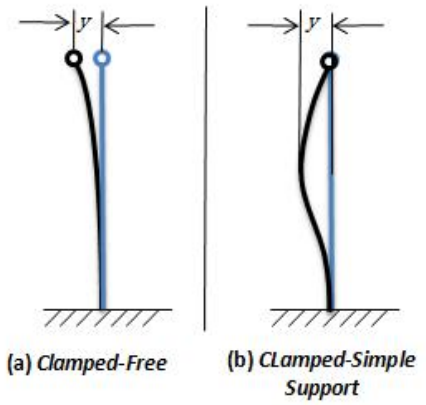

Figure 5.4: Illustration of deviation from ideal columns

ANSYS™ static structural platform was then used to simulate the load to induced buckling. The simulation for each clamped condition consisted of ten different loads, which was increased in even increments to determine the load under which *yielding of the material* was initiated in the simplified Rockprop.

The criteria that was used to determine this critical yield load P_{cr}, was the determination of the *load which caused the column material to start yielding.* This value was determined by taking cognisance of the FOS plot of the *Von-Mises* stress distribution at the overlap bond between the lower and upper columns (Fig. 5.5). This value for the *clamped-free* configuration was determined to be 240 kN and for the *clamped-simple* support configuration to be 260kN.

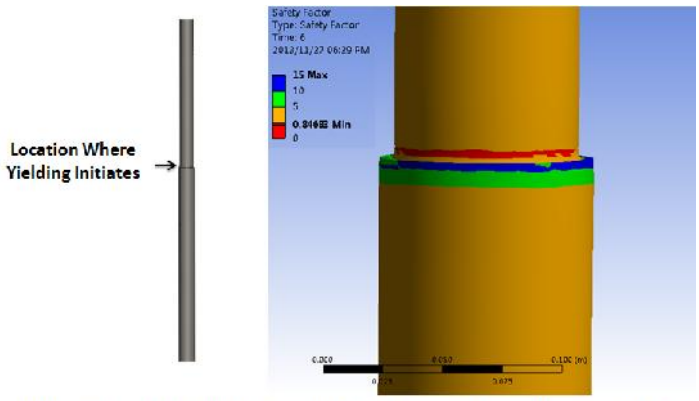

Figure 5.5: Factor of Safety Plot of the simulated Von-Mises stress distribution illustrating the location of yielding on one of the simulation models applicable to both configurations

To verify the obtained *Critical Load* P_{cr} calculations were carried based on *Buckling Theory* (Chapter 2.3) dictating the simplification to a so-called *equivalent column* consisting of the weighted averages of the diameters, thicknesses, Young's Moduli, and the yield strengths of the materials of the constituting bonded columns with a total length equal to the simulated bonded model L_T = 1.964 m for both configurations (Figure 5.1, Table 5.2).

Table 5.2: Parameters calculated for *equivalent column*

Description	Equivalent Value	
Young's Modulus *(E)*	207	GPa
Yield Strength *(σ_{yield})*	311	MPa
Wall thickness	5.5	mm
Outer diameter *(r_o)*	82.4	mm
Area *(A)*	1.33e-3	m^2
Moment of inertia of Area *(I)*	9.87e-7	m^{-4}
Length of column *(L_T)*	1964	mm

The *Euler and Johnson's buckling curves* (Fig. 5.6) were determined to evaluate the slenderness ratios of the different configurations and determine relevant buckling formula for the *Equivalent Column* (*EES* Calculations presented in Appendix B). The intersection of the *Euler and Johnson's* curves, at a slenderness ratio of 110.4, was determined from the Parametric Table (Appendix B) generated to determine the critical loads for the *Euler* and *Johnson* curves for effective column lengths of between 1.3 and 4 m. The corresponding effective length to this intersection is L_{eff} = 3.0 m.

For the *clamped-free* column configuration the critical buckling load was accordingly determined to be 131 kN based on its effective length of 3.93 using the Euler curve and for the *clamped-simple* support column configuration the critical buckling load is 374 kN based on its effective length of 1.37 m by using the Johnson's buckling curve (curve selection criteria as discussed in Chapter 2.3).

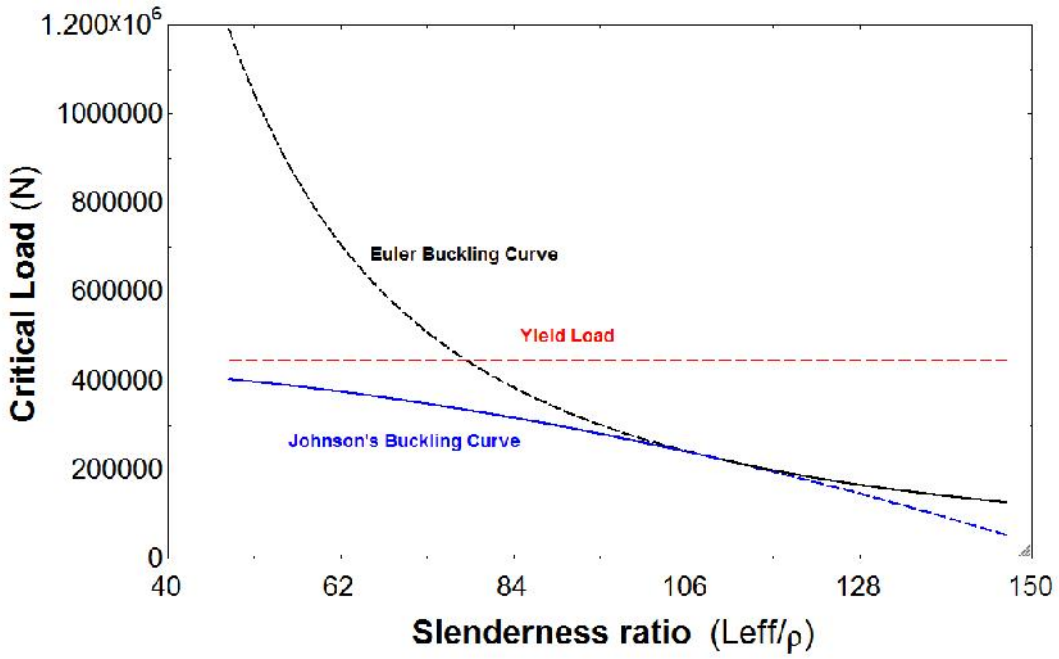

Figure 5.6: *Euler-Johnson's* curve for *equivalent column*

Table 5.3 presents a comparison between the critical loads that where calculated with the aid of *ANSYS™* simulations and the values calculated from the buckling principles as discussed in Chapter 2.3.

Table 5.3: Comparison between critical loads for different configurations

Description	***Clamped-free***		***Clamped-simple support***	
Effective length	3.93	m	1.37	m
***ANSYS™ Results:* Critical Load**	240	kN	260	kN
Equivalent column: Critical Load	131	kN	374	kN

The reason for the large difference between the results obtained from buckling theory and the results from the simulation is not clear although a number of reasons can be offered. The relative small difference between the critical loads obtained from the simulations for the two configurations may be attributed to a too low assumed deviation (y as discussed above) from the principal columnar axis. For both methodologies employed the results indicate that the critical load for the *clamped-simple* support is higher than that for the *clamped-free* support.

For the *clamped-simple support* configuration the *critical buckling load* is larger than the *yield - capability load*[3] (250 kN) of the prop under *quasi-static* conditions and therefore deduced to

[3] The yield capability load refers to the performance characteristic as described in Chapter 2.1.1 and is the value at which constant yielding is achieved.

carry out its function of supporting the excavated region while yielding with the expansion of the rock-mass without buckling.

For the *clamped-free* configuration it was deduced that buckling will occur at a load value that is less than the *quasi-static yield capability load* of the Rockprop MK2 under investigation and that consequently it will not under such conditions, perform its supporting and *yielding capability*. Rockprop MK2 has been applied in underground conditions and it has been observed to perform the mechanical function of support under *quasi-conditions* that can be described as static due to the prevailing Energy Release Rate. For this reason, and from the results discussed above, it is concluded that the *clamped-free* configuration does not apply.

5.2 Impact Buckling Response of Rockprop MK2 Support Prop Design

When seismic activities occur where Rockprops are installed, the columns are subjected to high velocity cyclic loading. This type of loading is associated with impact type loading on the columns and defined to be *dynamic loading conditions* (3m/s closure). This section presents the results of the associated investigation to determine the effect of this type of impact loading on the Rockprop in the *clamped-simple* support configuration, in order to determine the magnitude of the forces that need to be endured by Rockprop MK2 as a result.

To determine the buckling response of the Rockprop system an equivalent *spring mass damped* system (Fig.5.7) was used, where the two sections of the support are presented as two springs and two dampers in a series connection which for the approach presented in this section has been simplified to a system consisting of a single equivalent spring with stiffness $k_{equivalent}$ and damper with damping constant c. The equation of motion for this system is

$$m\ddot{x} + c\dot{x} + k_{equivalent}\, x = 0 \qquad (5.1)$$

where m = 25000 kg (the mass of the over-hanging rock that the column is designed to support), x is the displacement, $\dot{x}$ velocity and $\ddot{x}$ acceleration.

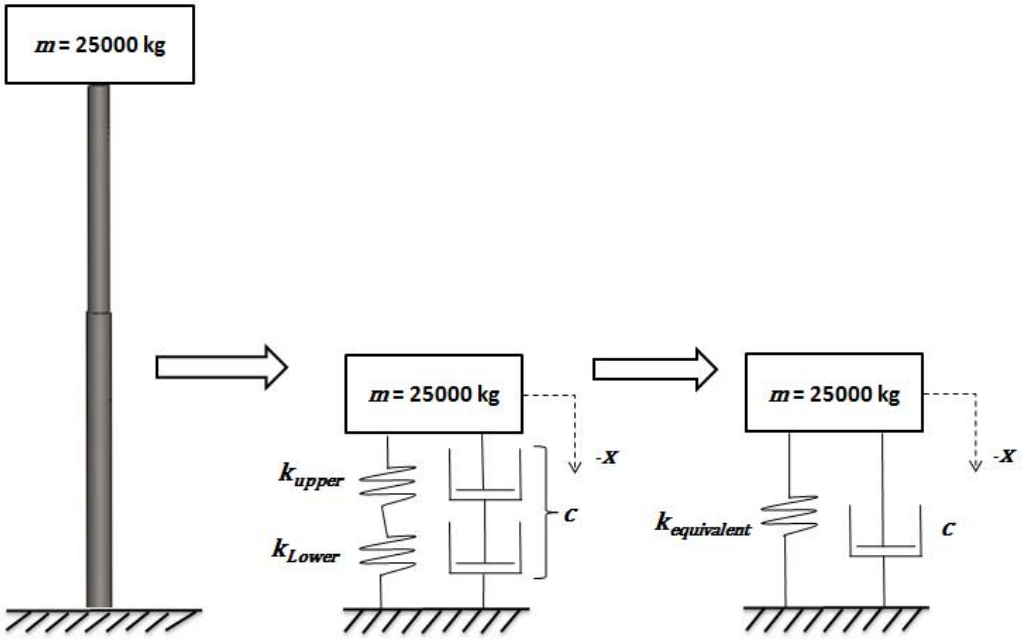

Figure 5.7: Spring-mass-damped system for Rockprop

To determine the stiffness $k_{equivalent}$, of the *equivalent column* a 3D model that was used for the simulation in Chapter 5.1 (for the *clamped-simple* configuration with the bonded column, Fig. 5.4b) was subjected a *ANSYS™ static structural* simulation for ten different loads to determine the downward displacement, x_s.(Fig. 5.8).

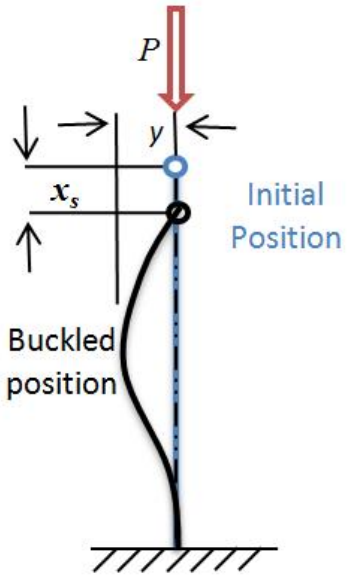

Figure 5.8: Buckling and axial displacements of a clamped simple supported column

The stiffness was then calculated using the relationship

$$k = \frac{\Delta P}{dx_s} \qquad (5.2)$$

The results obtained through this analysis and the average stiffness for the bonded column are presented in Table 5.4.

Table 5.4: ™ FEA input loads, resulting displacements and the average stiffness of the *spring –mass-damped* Rockprop

Load (kN)	*Clamped-Simple Support*	
	Displacement (x_s) m	$k_{equivalent}$ kN/m
50	2.65 e-4	151
60	3.32 e-4	151
70	3.98 e-4	151
80	4.65 e-4	151
90	5.31 e-4	151
100	5.97 e-4	151
110	6.64 e-4	151
120	7.30 e-4	151
130	7.97 e-4	
Average Stiffness		151

The damping constant c was calculated using the *damping ratio* $\zeta = \frac{c}{c_c}$ where $c_c = 2\sqrt{km} = 2m\omega_n$ (Rao, S.S. 2011:159-160). Typical values for the *damping ratio* ζ are below 0.01 for the materials involved in this study (Ewins, 1984), and assumed to be 0.01 for this study.

The parameters obtained, as explained and summarized in Table 5.5, were then imported into equation 5.1 in order to define the equation of motion, for the *spring mass damped* system (Fig. 5.7), for further calculations. (All calculations were carried out with the aid of *MATLAB™* and the setup are presented in Appendix C)

Table 5.5: Spring-mass-damped system parameters

Description	Symbol	*Clamped-Simple support*	
Equivalent Stiffness	$k_{equivalent}$	151	MN/m
Mass	m	25000	kg
Damping constant	c	39	kN/m/s

The Ordinary Differential Equation Solver (ODE), *ODE23* routine provided in *MATLAB™* was used to determine and plot the response of the *spring mass damped* system where the mass are subjected to an initial downward velocity of $\dot{x}(0) = -3$ m/s (*dynamic* loading) and the initial displacement condition is $x(0) = 0$. (The *ODE23* routine is described in *MATLAB™ User Manual* and the setup to solve the equations for this investigation is given in Appendix C.)

The results of the calculations for the response for the *Clamped Simple* support configuration (Fig. 5.3 (b)), subjected to the conditions described above is presented in Figure 5.9.

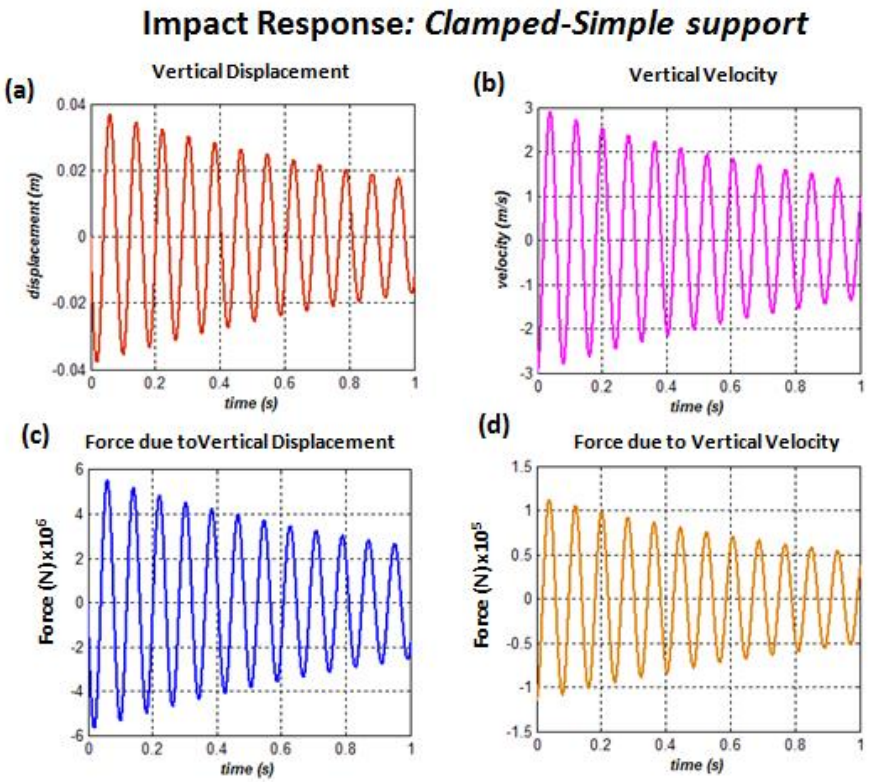

Figure 5.9: Response of spring-mass-damped system in *Clamped-Simple support* configuration

Figure 5.9 (a) presents the vertical displacement of the top end of the column as a result of the impact load while the associated vertical velocity, simultaneously experienced by the top end of the column, is presented by Figure 5.9(b). The initial conditions of $\dot{x}(0) = -3$ m/s and $x(0) = 0$ can be confirmed from these graphs. Figure 5.9 (c) present the force experienced by the column due to the vertical displacement while the force experienced due to the vertical velocity is presented in Figure 5.9 (d). The resultant of these forces at the moment of maximum magnitude was then obtained in order to determine the effect of the force on the buckling potential and performance of the Rockprop.

The maximum resultant force F_{MAX} experienced due to the displacement and velocity components was calculated through population of

$$F_{MAX} = \sqrt{(k_e X)^2 + \left(c\dot{X}\right)^2} \qquad (5.3)$$

where X is the vertical displacement experienced and $\dot{X}$ is the velocity at time t when the resultant force has a maximum magnitude. The frequencies of the responses presented were confirmed by comparing the frequencies on the graphs with the calculated values obtained by evaluating:

$$f = \frac{\omega_n}{2\pi} \qquad (5.4) \quad \text{and} \quad \tau = \frac{1}{f} \qquad (5.5)$$

where f is the frequency of the response, ω_n is the natural frequency and τ is the period of a cycle. The result of this calculation is presented in Table 5.6. (Further detail of approach is presented in Appendix C)

Table 5.6: Maximum force experienced by Rockprop MK2due to dynamic impact of 3m/s

Description	Symbol	*Clamped-Simple support*	
Frequency	f	12.33	Hz
Maximum vertical Displacement	X	38.1	mm
Time of maximum force	t	0.020	s
Maximum Force Experienced	F_{MAX}	5.73	MN

The frequencies presented in Table 5.6 and the frequencies from the graphs are equal which is an indication of a good solution obtained from the *MATLAB™* ODE23 routine.

5.3 Conclusion of Buckling study

One of the aims of this study was to investigate the theoretical potential of buckling on the column and the implications that buckling may have on the performance of the support unit. The Rockprop MK 2 with a maximum height of 2.1 m was chosen for this study and a comparison was made between two different configurations of buckling. These where: a *clamped-free* configuration and a *clamped-simple support* configuration.

A static buckling analysis was carried out to determine the theoretical critical load of the column for the two chosen configurations. For a *clamped-free* configuration it was determined that buckling may occur at a load lower than the designed *yield capability load* of the Rockprop. This implies that if a *clamped-free* configuration prevailed the column would fail due to buckling and that if would not perform its mechanical function of supporting the excavated region while yielding with the elastic expansion of the rock-mass.

If a *clamped-simple support* configuration prevails, the critical buckling load is larger than *yield capability load* which implies that yielding of the lower column would occur and the Rockprop can carry out its function of supporting the excavated region while yielding with the expansion of the rock-mass.

A dynamic buckling analysis was carried out to determine the effect of an impact load on the Rockprop. This theoretical evaluation was required to determine the response or behaviour of Rockprop MK2 due to seismic activities and rock burst conditions which are regular events in stopes where these types of support are employed. The impact load was set at a momentary initial downward velocity of the mass of 3m/s (the design standard required for prop supports) and the response was simulated in a *MATLAB™* ODE23 routine. The maximum force that is experienced by the column due to the impact load was then calculated from equation of motion response graphs (Fig 5.9). For this dynamic buckling analysis employing the methodology described it was found that the impact force massively exceeds the *yield load*[4], *yield capability loads* and *critical loads*[5] for a *Clamped-simple support* condition, and that the column will fail catastrophically.

[4] Axial load that causes stresses in the material of the column to exceed their yield limit stress.
[5] Load that causes failure due to buckling.

CHAPTER 6 Summary

Chapter 6 reviews and discusses the conclusions that are drawn from the results of this study and aligns these in terms of the aim of the study. It also presents recommendations for further work.

6.1 Conclusions and Discussion

In Chapter 1.2 a problem statement is presented and the aim of the study divided in four main components. The first aim was to review the design base, design principles and performance requirements of stope support technologies. A comprehensive background study, presented in Chapter 2.1, summarizes the rock mechanics involved, types of support that are used in stope operations as well as their performance characteristics followed by a discussion on mechanical types of support units. It was concluded that the current method of design consist of an elaborate *trial and error* process that is time consuming and expensive.

Software simulation processes used in the design phases of components and assemblies to minimize the expensive and time consuming nature associated with *trial and error* design processes. The second aim of the study therefore was to review the possible application of computer simulations to a stope support design. Little information and examples of the application of this methodology was found.

The third aim of the study was to determine the feasibility of the application of *Finite Element Modelling (FEM)* to the deformation of modern support units under specified conditions. A comprehensive literature review (Chapter 2.2) was also undertaken to determine the fundamentals that are associated with this type of *FEM* procedure.

To determine the application feasibility of the intended analysis, a chosen commercial support design was available, and from findings in the literature review it was decided to use the simulation code provided by *ANSYS™* as the principal *FEM* software.

The following conclusions are drawn from the results of the *ANSYS™* simulations presented in Chapter 4.

1. The trend of the simulated performance curves for *dynamic* closure condition resemble the trend of performance curves obtained from laboratory testing (when adequate equipment was still available to test props under *dynamic* conditions) (Fig 2.4) of models different to the Rockprop MK 2, and the required curve for a constant *yielding capability* that the Rockprop is designed to achieve.
2. Although dynamic modelling was successfully undertaken and shown to be feasible as the results of the simulation were found to be in accordance with the solution provided by an independent *axi-symmetric* simulation that was also carried out, based on an

assumed *friction factor*, a refined value of the constant *yield capability load* can only be obtained if physical empirical testing is undertaken in future to determine the actual value of the *friction factor*.

3. From the results of the *dynamic* closure rate simulations, it is evident that a friction factor of approximately 0.2 is required for the Rockprop MK 2 to be able to carry a constant yield load of 250 kN. From the results for the *quasi-static* closure rate simulations, it is evident that that the actual friction factor varies between 0.07 and 0.1 for *quasi-static* load rates. Based on the exponential decay curve for the friction factor vs. the relative contact velocity between surfaces (Fig. 2.16) it can be concluded that the *friction factor* for *dynamic* conditions is approximately equal to, or less than the friction factor for *quasi static* conditions. This implies that the constant yield capability of the Rockprop under *dynamic* closure conditions is at most 175 kN or less and inevitably lower than the design specification of 250 kN.

The fourth and final aim of this study was to determine the theoretical potential of buckling on a specific commercially available stope support design and the implications that it may have on the performance of the prop. A comprehensive literature review was accordingly carried out to determine the elements that are required to evaluate buckling in such columns. This review is presented in Chapter 2.3. The buckling analysis, presented in Chapter 5, was carried out using a combination of buckling theory and *FEA* simulations on a *clamped-simple support* configuration and a *clamped-free* configuration with the results compared.

From the buckling analysis it was concluded that:

1. For a *clamped-simple support* configuration subjected to *static* loading conditions it was found that the critical *buckling load* exceeds the *yield capability load* of the column and that consequently the prop can perform its mechanical function without buckling that otherwise influence continued performance.
2. For a *clamped-free* configuration subjected to *static* loading conditions it was concluded that the *critical buckling load* is less than the *yield capability load* of the column which implies that the prop will buckle and that it would not be able to further perform its mechanical function.
3. From the evaluation of the available design subjected to *dynamic* loading conditions (which were defined to be impact loading with an initial velocity of 3m/s) for the *clamped-simple support* condition that was found to be applicable, it was concluded that the prop would experience excessive forces and that these forces exceed the *yield loads, yield capability loads and critical buckling loads* of the column and it was concluded that catastrophic failure occurs during these loading conditions.

In summary this study proved that it is possible to simulate the performance curve of a friction prop design provided that the correct information regarding friction between the mating surfaces of the prop and material properties of the design are known. It also presents a methodology to investigate the theoretical effect of high velocity impact loading on the buckling characteristics of friction prop designs and of slender columns in general which is highly applicable to these types of supports. The methodologies employed will contribute to improving the design and development costing of such supports which are currently carried out in an empirical manner.

6.2 Recommendations

The current study revealed that there are opportunities for further development and associated studies to be conducted in this field. Recommendations for further work include the following:

- A study to determine the friction behaviour and exact friction factors between the deformation wedge and the lower column for different load rates. With the friction factor known, it is thought that more accurate simulations could be conducted for various closure conditions that would improve on effectiveness in practice of prop designs.
- High strain rate influences the mechanical properties of the steels that are used (especially in the non-linear mode). A study should be conducted to determine the magnitude of this phenomenon on the results of this work with respect to *dynamic* loading of prop supports in order to select the best material model setup forthis particular application.
- It is thought that a study needs to be undertaken to improve the damping capability of such props in general in order to further enhance prop support capabilities under dynamic conditions.

Bibliography

ANSYS™ 13.0, User Guide

BANDIS, S., LUMSDEN, A.C. & BARTON, N.R. 1981. Experimental studies of scale effects on the shear behaviour of rock joints. International journal of rock mechanics and mining sciences and, 18(1):1-21.

BANDIS, S.C., LUMSDEN, A.C. & BARTON, N.R. 1983. Fundamentals of rock joint deformation. International journal of rock mechanics and mining sciences and, 20(6):249-268.

BARCZAK, T.M., 2005. AN OVERVIEW OF STANDING ROOF SUPPORT PRACTICES AND DEVELOPMENTS IN THE UNITED STATES. National Institute fro Occupational Safety and Health.

BEAKOU, A., CANO, M., CAM, J.-.L. & VERNEY, V. 2011. Modelling slit tape buckling during automated prepreg manufacturing: A local approach. Composite structures, 93(10):2628-2635.

BORESI, A.P. & SCHMIDT, R.J. 2003. Adcanced mechanics of materials. Sixth Edition ed. United States of America: John Wiley & Sons, Inc. 681-104-146p.

BORESI, A.P. & SCHMIDT, R.J. 2003. Advanced mechanics of materials. Sixth Edition ed. United States of America: John Wiley & Sons, Inc. 681-8-16p.

BRACKEBUSCH, F. 1992. Underground mining: Supported methods. (In Karmis, M., ed. Sme mining engineering handbook. VOLUME 2 ed. United States of America: Society for Mining Metalurgy and Exploration INC. p. 1741-1743-1777.).

BRADY, B.H.G. & BROWN, E.T. 1993. Rock mechanics for underground mining. Rock mechanics for underground mining, .

BUDAVARI, S. 1983. Response of the rock mass to excavations underground. Rock mechanics in mining practice, 555-76.

COOK, N.G.W., HOEK, E., PRETORIUS, J.P.G., ORTLEPP, W.D. & SALAMON, M.D.G. 1966. Rock mechanics applied to the study of rockbursts. J.S.afr.inst.min.metall., 66(10):435-528.

DAEHNKE, A. 2001. Addressing the variability of elongate support performance. Journal of the south african institute of mining and metallurgy, 101(2):83-90.

DAEHNKE, A., SALAMON, M.D.G. & ROBERTS, M.K.C. 1999. Investigating zones of support influence and quantifying stable hangingwall spans between support units. J.of south african inst.of mining and metall.

DAEHNKE, A., VAN ZYL, M. & ROBERTS, M.K.C. 2001. Review and application of stope support design criteria. Journal of the south african institute of mining and metallurgy, 101(3):135-164.

EVANS, W.H. 1941. The strength of undermined strata. Trans.inst.min.metall., 50(50):475-532.

EWINS, D.J. 1984. Modal Testing. Theory, practice and application. Second Edition.

HAYCOCKS C 1992. Stope and pillar mining. (In Hartman, H.L., ed. Sme mining engineering handbook. 2nd ed. United States of America: Society of Minig Metallurgy and Exploration Inc. p. 1702-1702-1711.).

HEDLEY, D.G.F. 1992. Rockburst handbook for ontario hardrock mines. Rockburst handbook for ontario hardrock mines, .

HIBBELER, R.C. 2005. Mechanincs of materials. Sixth Edition ed. Upper Saddle River, New Jersey 07458: Pearson Prentice Hall. 873-3-83p. (International edition.).

HINDLEY, M. 2011. Verbal communication with author. ESKOM RT&D.

JOHNSON, G.R., COOK, W.H. 1983. A Constitutive Model and Data for Metals Subjected to Large Strains,High Strain Rates and High Temperatures, Proceedings of the 7th International Symposium on Ballistics, The Hague, The Netharlands.

JUVINALL, R.C. & MARSHEK, K.M., eds. 2006. Fundamentals of machine component design. Fourth Edition ed. John Wiley & Sons (Asia) Pte Ltd. 764.

KIM, N. & CHOI, D. 2011. Inelastic static and dynamic stability analyses of a column subjected to a nonconservative force. Mechanics based design of structures and machines, 39(3):346-366.

LOGAN, D.L. 2002. A first course in finite element method. Third Edition ed. USA: Brooks/Cole. 696p.

M.D.G., S. 1970. Stability, instability and design of pillar workings. International journal of rock mechanics and mining sciences & geomechanics abstracts, 7(6):613-631.

MAC DONALD, B.J. 2011. Practical stress analyses with finite elements. Dublin: Glasnevin Publishing. 388p.

MAC DONALD, B.J. 2007. Practical stress analyses with finite elements. Dublin: Glasnevin Publishing. 350p.

MCMAHON, T. 1988. Rock burst research and the coeur d'alene district. Bureau of mines information circular.

MITRI, H.S., TANG, B. & SIMON, R. 1999. FE modelling of mining-induced energy release and storage rates. Journal of the south african institute of mining and metallurgy, 99(2):103-110.

ORLANDO, D., GONC¸ALVES, P.B., REGA, G. & LENCI, S. 2011. Influence of modal coupling on the nonlinear dynamics of Augusti's model. Journal of computational and nonlinear dynamics, 6(4):041014-041014-11.

ORTLEPP, W.D. 1983. Considerations in the design of support for deep hard-rock tunnels. (In Anon. Proceedings - 5th congress of the international society for rock mechanics. 1983. A. A. Balkema. p. D179-D187.).

PRETORIUS, M.J. 1999. A mathematical model to quantify stope support reaction. Proceedings of the 2nd southern african rock engineering symposium, 204-215.

RAO, S.S. 2011. Mechanical vibrations. Fifth Edition ed. New York: Pearson Prentice Hall. 1077p.

REDDY, J.N. 2006. An introduction to the finite element method. Third Edition ed. New York: Mc Graw-Hill. 755p.

ROBERTS, M.K.C., DAEHNKE, A. & JAKU, E.P. 2001. Rock-related fatality trends in the south african gold mining industry. Journal of the south african institute of mining and metallurgy, 101(7):353-358.

ROBERTS, M.K.C., JAGER, A.J. & RIEMANN, K. 1987. The performance characteristics of timber props. Chamber of mines report, 35.

SALAMON, M.D.G. 1993. Some applications of geomechanical modelling in rockburst and related research. Rockbursts and seismicity in mines, 297-309.

SALAMON, M.D.G. 1984. Energy considerations in rock mechanics: Fundamental results. Journal of the south african institute of mining and metallurgy, 84(8):233-246.

SALAMON, M.D.G. 1983. Linear models for predicting surface subsidence. (In Anon. Proceedings - 5th congress of the international society for rock mechanics. 1983. A. A. Balkema. p. E107-E114.).

SALAMON, M.D.G. 1983. Rockburst hazard and the fight for its alleviation in south african gold mines. Proceedings of rockburst prediction and control, 11-36.

SALAMON, M.D.G. 1974. Rock mechanics of underground excavations. Advance in rock mechanics, 1 B951-1099.

SALAMON, M.D.G. 1970. Stability, instability and design of pillar workings. International journal of rock mechanics and mining sciences and, 7(6):613-631.

WAGNER, H. 1984. Support requirements for rockburst conditions. (In Anon. 1984. p. 209-218.).

WALSH, J.B. 1977. Energy changes due to mining. International journal of rock mechanics and mining sciences and, 14(1):25-33.

APPENDIX A: Calculation to determine the Tangent Modulus for AISI 1010

$$E_{Tan} = \frac{\pm_U - \pm_Y}{£_{fail} - £_{proof}}$$

where: σ_U is the ultimate stress of the material

σ_Y is the yield stress of the material

ε_{fail} is the material failures strain

ε_{proof} is the proof strain (assumed to be 0.002) of the material. In other words amount of strain that will be recovered when the load is released.

These values and the results is presented in the table below:

Description	Symbol	Value
Yield Strength	σ_y	299 MPa
Ultimate Tensile Strength	σ_u	409 MPa
Elongation	*El*	43 %
Modulus of Elasticity	*E*	200 GPa
Tangent Modulus	E_{tan}	2682 MPa

APPENDIX B: Euler and Johnson Buckling Analyses

This Appendix presents the EES code that was used to determine which of the buckling formulae the best for the specific column is:

Buckling calculations for the Rockprop MK2 Equivalent Column

Calculate the Critical Load for centre loaded columns based on the EULER FORMULA

Equivalent column

$$P_{cre} = \pi^2 \cdot E_e \cdot \frac{I_e}{L_e^2}$$ p439BoresiScmidt

$$E_e = 2.07 \times 10^{11}$$

$$I_e = \pi \cdot \frac{r_{oe}^4}{4} - \pi \cdot \frac{r_{ie}^4}{4}$$

$L_e = 1.964$

Length of column

$$L_{effe} = L_e$$

$$r_{oe} = \frac{0.0824}{2}$$

$t_e = 0.0055$ [m]

$$r_{ie} = r_{oe} - t_e$$

Calculate the Critical Load for ideal columns based on the JOHONSON FORMULA

$$P_{crjoe} = S_{ye} \cdot \left[1 - \frac{S_{ye}}{4 \cdot \pi^2 \cdot E_e} \cdot \left(\frac{L_{effe}}{k_e}\right)^2\right] \cdot A_e$$

$$S_{ye} = 3.35 \times 10^8$$

$$A_e = \pi \cdot r_{oe}^2 - \pi \cdot r_{ie}^2$$

$$k_e = \sqrt{\frac{I_e}{A_e}}$$

$$Slendernessratio_e = \frac{L_{effe}}{k_e}$$

$$P_{eyield} = S_{ye} \cdot A_e$$

For these calculations the length was altered for each formula and the values plotted to achieve the comparison curve. The table is presented below.

1..28	1 L_e	2 P_{cre}	3 P_{crjoe}	4 P_{eyield}	5 Slendernessrati
Run 1	1.3	1.193E+06	403621	445127	47.69
Run 2	1.4	1.029E+06	396990	445127	51.36
Run 3	1.5	896407	389868	445127	55.03
Run 4	1.6	787857	382254	445127	58.7
Run 5	1.7	697894	374150	445127	62.37
Run 6	1.8	622505	365554	445127	66.04
Run 7	1.9	558702	356467	445127	69.71
Run 8	2	504229	346889	445127	73.37
Run 9	2.1	457350	336819	445127	77.04
Run 10	2.2	416718	326259	445127	80.71
Run 11	2.3	381269	315207	445127	84.38
Run 12	2.4	350159	303664	445127	88.05
Run 13	2.5	322706	291630	445127	91.72
Run 14	2.6	298360	279104	445127	95.39
Run 15	2.7	276669	266088	445127	99.05
Run 16	2.8	257260	252580	445127	102.7
Run 17	2.9	239823	238581	445127	106.4
Run 18	3	224102	224091	445127	110.1
Run 19	3.1	209877	209110	445127	113.7
Run 20	3.2	196964	193637	445127	117.4
Run 21	3.3	185208	177674	445127	121.1
Run 22	3.4	174474	161219	445127	124.7
Run 23	3.5	164646	144273	445127	128.4
Run 24	3.6	155626	126835	445127	132.1
Run 25	3.7	147328	108907	445127	135.7
Run 26	3.8	139676	90487	445127	139.4
Run 27	3.9	132605	71576	445127	143.1
Run 28	4	126057	52174	445127	146.7

APPENDIX C: MATLAB ODE23 Procedure for Buckling Analyses

The buckling response of the columns under impact load was calculated using ODE 23. This Appendix presents the code that was used for each column with its ODE23 execution.

Ordinary differential equations (ODE's) can be solved using different variances of Runge-Kutta numerical integration methods. *MATLAB™* provides a routine, called the *ODE23* that uses a combination of the second- and third order Runge-Kutta methods to solve equations for variable time steps. It is designed to solve the general equation:

$$\frac{dx}{dt} = f(t,x) \qquad x(t_0) = x_0$$

where t is the independent variable and x is the vector dependant of variables to be found. Initial conditions must be specified to be able to solve the equation. This is a value for x_0 at t_0.

Clamped-Simple Support Configuration

```
function w = CombinedColumn(x0)
%Initial Values
%   Combined Columns Buckling

Kc = 1.51e8;
m = 25000;
c = 0.01*2*sqrt(Kc*m);

omegac = sqrt(Kc/m);
tauc = 2*pi/omegac;
fc = 1/tauc;



% Execution of Runge-Kut

w = 1;
tspan = [0:0.0001:20];

[t,x] = ode23('combinedcolumns',tspan,x0);

dx = x(:,1);
ddx = x(:,2);

% ddx = pi^2*x(:,2)/(4*ll);
% dddx = omegal^2*ddx;
Fdx = Kc*dx;
```

```
Fddx = c*ddx;
Ftot1 = Fdx+Fddx;
% Fddx = Fddx';
Ftot = sqrt(Fdx.^2+Fddx.^2);


subplot(2,3,1);
plot(t,x(:,1));
grid on
title('Vertical Displacement');
xlabel('time (s)');
ylabel('displacement (m)');
subplot(2,3,2);
plot(t,x(:,2));
grid on
title('Vertical Velocity');
xlabel('time (s)');
ylabel('velocity (m/s)');
subplot(2,3,3);
plot(t,Fdx);
grid on
title('Force due to Vertical Displacement');
xlabel('time (s)');
ylabel('displacement (m)');
subplot(2,3,4);
plot(t,Fddx);
grid on
title('Force due to Vertical Velocity');
xlabel('time (s)');
ylabel('velocity (m/s)');
subplot(2,3,5);
plot(t,Ftot);
grid on
title('Vertical Force');
xlabel('time (s)');
ylabel('force (N)');
subplot(2,3,6);
plot(t,Ftot1);
grid on
title('Fx+F?');
xlabel('time (s)');
ylabel('force (N)');

end
```

ODE23 Routine

```
function f = combinedcolumns(t,x)

m = 25000;
Kc = 1.51e8;                %Stiffness of combined columns
c = 0.01*2*sqrt(Kc*m);   %Viscous damping constant for combined columns

omegac = sqrt(Kc/m);   %Natural frequency of combined columns
```

```
tauc = 2*pi/omegac;
fc = 1/tauc;



f = zeros (2,1);
f(1) = x(2);
f(2) = (-Kc/m)*x(1)-(c/m)*x(2);

end
```

Clamped-Free Configuration

```
function w = CombinedColumn_Clamped Free(x0)
%Initial Values
%   Combined Columns Buckling

Kc = 148e6
m = 25000
c = 0.01*2*sqrt(Kc*m)

omegac = sqrt(Kc/m)
tauc = 2*pi/omegac
fc = 1/tauc



% Execution of Runge-Kuta

w = 1;
tspan = [0:0.0001:20];

[t,x] = ode23('combinedcolumns_CF',tspan,x0);

dx = x(:,1);
ddx = x(:,2);

% ddx = pi^2*x(:,2)/(4*ll);
% dddx = omegal^2*ddx;
Fdx = Kc*dx;
Fddx = c*ddx;
Ftot1 = Fdx+Fddx;
% Fddx = Fddx';
Ftot = sqrt(Fdx.^2+Fddx.^2);
```

```
subplot(2,3,1);
plot(t,x(:,1));
grid on
title('Vertical Displacement');
xlabel('time (s)');
ylabel('displacement (m)');
subplot(2,3,2);
plot(t,x(:,2));
grid on
title('Vertical Velocity');
xlabel('time (s)');
ylabel('velocity (m/s)');
subplot(2,3,3);
plot(t,Fdx);
grid on
title('Force due to Vertical Displacement');
xlabel('time (s)');
ylabel('displacement (m)');
subplot(2,3,4);
plot(t,Fddx);
grid on
title('Force due to Vertical Velocity');
xlabel('time (s)');
ylabel('velocity (m/s)');
subplot(2,3,5);
plot(t,Ftot);
grid on
title('Vertical Force');
xlabel('time (s)');
ylabel('force (N)');
subplot(2,3,6);
plot(t,Ftot1);
grid on
title('Fx+F?');
xlabel('time (s)');
ylabel('force (N)');


end
```

ODE23 Routine

```
function f = combinedcolumns_CF(t,x)

m = 25000;
Kc = 148e6;                %Stiffness of combined columns
c = 0.01*2*sqrt(Kc*m);   %Viscous damping constant for combined columns

omegac = sqrt(Kc/m);   %Natural frequency of combined columns
tauc = 2*pi/omegac;
fc = 1/tauc;



f = zeros (2,1);
```

```
f(1) = x(2);
f(2) = (-Kc/m)*x(1)-(c/m)*x(2);

end
```